European Polymer Journal 220 (2024) 113455

Contents lists available at ScienceDirect

European Polymer Journal

journal homepage: www.elsevier.com/locate/europolj

Tailoring copolymer architectures and macromolecular interactions for enhanced nanotherapeutic delivery: A design-by-architecture approach

Ilaria Porello, Federico Stucchi, Giulia Sbaruffati, Francesco Cellesi *

Department of Chemistry, Materials and Chemical Engineering "G. Natta", Politecnico di Milano, Via Luigi Mancinelli 7, 20131, Milan, Italy

ARTICLE INFO

Keywords:
Polymeric nanoparticles
Functional copolymers
Drug nanodelivery
Polymers architecture
Macromolecular interactions
Thiolated nanocarriers

ABSTRACT

Amphiphilic copolymers with precise macromolecular topologies are crucial in nanomedicine for enhancing drug delivery by improving solubilization, stabilization, and therapeutic efficacy on target tissues. This study employs a design-by-architecture approach to identify factors influencing interactions between synthesized macromolecules and biological systems for optimal drug nanodelivery. Copolymers combining poly(ε-caprolactone) blocks and poly(polyethylene glycol methacrylate) or poly(glycerol methacrylate), were synthesized to investigate how architectural adjustments impact self-assembly, nanoparticle size, drug loading, and biomolecule interactions. Linear and brush block copolymers with varied block lengths were studied for their self-assembly behavior in aqueous environments. Both copolymer types formed smaller nanoparticles with extended hydrophilic blocks, with brush block copolymers showing superior performance due to their peculiar macromolecular architecture. Incorporating 'clickable' glycidyl units within the hydrophilic block minimally affected particle size. Controlled functionalization with thiol groups resulted in stable nanoparticles with enhanced size reduction and mucoadhesive properties, potentially improving targeted drug delivery and therapeutic effects.

1. Introduction

In recent years, biocompatible amphiphilic copolymers with complex, well-defined macromolecular topologies and specific functionalities have shown promising applications in nanomedicine as drug delivery tools [1–7], enhancing drug solubilization and stabilization [8–11] to maximise curative effects on targeted tissues [12–14].

While nanoparticles derived from linear (co)polymers often lack precise property control, advanced macromolecular designs, which independently control architectural parameters, can offer a broader range of features in self-assembly, final physicochemical properties (such as nanoparticle size, shape [15], surface topography [16], and drug loading), and bioactivity (including protein adsorption, biodistribution, cell interaction, and drug release profile) [8,17–20]. Inspired by nature and the advanced features of biomacromolecules (such as nucleic acids and proteins), precision chemistry tools have been developed to prepare synthetic macromolecules with unprecedented properties, and more recently, to achieve the structural and functional complexity of sequence-defined polymers [21,22].

Controlled living polymerization techniques, including Ring Opening Polymerization (ROP) [23,24] and Atom Transfer Radical Polymerization (ATRP) [25,26], allow the synthesis of biocompatible copolymers with predetermined molecular weights, composition, and controlled topologies (linear, multi-arm, comb-like, brush block) [1,27–30]. Combining these polymerization tools with post-functionalization via click-chemistry reactions ensures the production of multifunctional nanocarriers with customized properties, such as the ability to cross biological barriers and target specific cells, tissues, and organs [25,31], maximizing efficacy and selectivity while reducing side effects [32–37].

Advancing nanomedicine involves overcoming several obstacles, including opsonization, nonspecific uptake by immune cells and organs, and the challenge of penetrating target tissues and cells. The physical phenomena governing nanoparticles performance against these physiological barriers are not fully understood due to the lack of comprehensive descriptions of the physicochemical principles necessary for rational nanocarrier design [38], which are crucial to define efficacious interactions with biological systems [39]. Moreover, targeting at a cellular/molecular level remains one of the major challenges in biomedical treatments. In this regard, the presence of active functional groups within nanoparticle structures plays a fundamental role in governing interactions with biological environments *in vitro* and *in vivo*.

* Corresponding author.
E-mail address: francesco.cellesi@polimi.it (F. Cellesi).

https://doi.org/10.1016/j.eurpolymj.2024.113455
Received 24 July 2024; Received in revised form 8 September 2024; Accepted 11 September 2024
Available online 12 September 2024

Therefore, a deeper understanding of their action mechanism is decisive to effectively select them and to reach the required nanodelivery performances [40].

This work presents a design-by-architecture approach to identify key factors crucial to achieve efficient interactions between synthesized macromolecules and target biological systems, aiming for optimal drug nanodelivery. These factors include independently adjustable architectural parameters such as main polymer chain and side chains length, number of arms/branches, type of monomeric units and their molar ratios, and density and position of bioactive moieties. Precise control over nanoparticle size, shape, and active targeting may ensure to finely predict *in vivo* behaviour, ensuring to cross the biological barriers, to avoid premature clearance from the body, maintaining adequate residence time in the target tissue, and achieving controlled drug release. Through this approach, we aim to provide evidence for proof-of-mechanisms, rather than creating complex polymer systems solely for proof-of-concept feasibility [41,42], focusing on how polymer design and synthesis could lead to optimized physicochemical properties of the resulting material.

A library of amphiphilic copolymers based on hydrophobic, biodegradable poly(ε-caprolactone) (PCL) blocks and hydrophilic poly(polyethylene glycol methacrylate) P(PEGMA) or poly(glycerol methacrylate) (PGMA) was synthesized *via* a combination of ROP and ATRP techniques respectively [43–45]. These reactions have proven to be highly versatile and can be easily optimized in terms of sustainability and E-factor. They allow to select easily recyclable organic solvents (as in the case of ATRP) or to conduct bulk synthesis (as done for all ROPs presented), while also minimizing the amount of catalyst and reactivating it by means of reducing agents (as performed for AGET ATRP) [46].

Different polymeric architectures (linear, comb-like, and brush-block), chain lengths (degree of polymerization), and monomer types were rationally selected to evaluate how polymer design parameters affect self-assembly in aqueous suspensions. Indeed, these materials are able to form colloidal nanosystems (micelles) which typically exhibit a core–shell morphology, where lipophilic drugs can be physically entrapped into the hydrophobic and biodegradable PCL core [47,48]. The hydrophilic P(PEGMA)/PGMA chains provide steric repulsion and colloidal stability, along with reduced immune recognition and enhanced blood circulation time after administration [17,49–53].

While P(PEGMA) is commonly used in nanomedicine for its biocompatibility, hydrophilicity, and ability to form stealth nanoparticles that can evade the immune system, PGMA has recently received attention as an alternative to PEG due to its low toxicity, limited interactions with proteins, and high hydrophilicity, which minimize immune recognition [54–57].

The hydrophilic PEGMA or GMA monomers were copolymerized with glycidyl methacrylate (gMA) to achieve 'click' functionality for post-functionalization. The epoxide ring opening of the gMA units by thiolated compounds is a valuable strategy for conjugation, given its high yield and quantitative conversion under stoichiometric conditions [58,59].

Based on this strategy, functionalizable polymeric micelles can be obtained, which are useful for delivering various therapeutics depending on the desired application.

Due to the broad versatility and biocompatibility of the selected polymerization reactions, it would be possible to achieve different nanomaterials with analogous functions by changing the chosen precursors (such as monomers and functional units) according to the specific characteristics required for the final product.

Doxorubicin (DOX) was chosen as a model drug to evaluate the encapsulation performances of the different series of copolymers. DOX is a frontline chemotherapeutic agent used to treat various cancers, including carcinomas, sarcomas, and hematological malignancies. Despite its widespread clinical use, nanoencapsulation is frequently necessary due to its significant cardiac toxicity and short half-life, which can limit its therapeutic effectiveness [60].

In this study, glycidyl groups were functionalized with thioacetic acid to provide the macromolecular structure with protected thiols in form of thioacetic esters, which can be deprotected under selective base-catalyzed hydrolysis [61,62]. The degree of functionalization was varied by changing the number of glycidyl units added during polymerization to evaluate how this affects nanoparticle properties, behavior, and

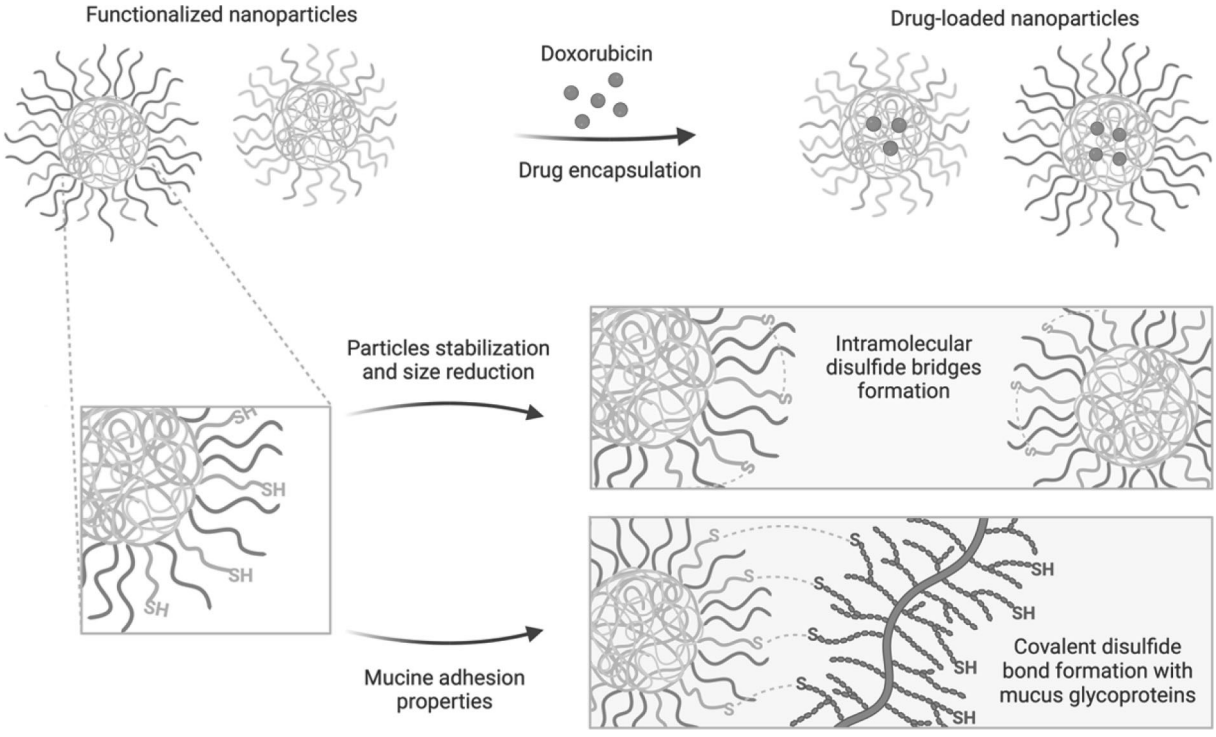

Fig. 1. Schematic representation of nanoparticles formulation and drug loading process (top) and potential mucoadhesive application of thiol functionalization (bottom). Image created with Biorender.com.

interactions with biological systems. Thiol functionalization has been extensively studied due to its versatility and broad benefits [63–67]. Thiolated polymers can form disulfide cross-links, either in the nanoparticle core or outer shell, thus improving stability, and preventing early drug release. Disulfide bridges formation also offers the advantage of producing smaller nanoassemblies with narrower size distribution due to the formation of intramolecular network [68,69]. Thiolated polymers and nanocarriers have also been used to increase the mucoadhesive properties of several drug delivery systems due to their ability to form covalent bonds with cysteine-rich subdomains of mucus glycoproteins [40,70–73]. Under physiological conditions, a disulfide-thiol exchange process can occur, mimicking the natural bonds formed within the mucosal layer, which are stronger than the non-covalent interactions formed by non-thiolated polymers [70,74–76].

Based on this consideration, we investigated how the formation of disulfide bridges between the functionalized chains in the nanoparticles shell may enhance particles size reduction and mucoadhesive properties, potentially improving targeted drug delivery and therapeutic effects. *In vitro* tests were carried out to evaluate the ability of these nanocarriers to interact with mucins from porcine gastric mucus [72], depending on their different degrees of functionalization. The interaction between thiolated macromolecules and bovine serum albumin (BSA) was also investigated, in order to evaluate if the presence of thiols along the polymer structure may alter the interaction with BSA via its cysteine residues, thus inducing undesirable protein adsorption in biological fluids.

A schematic representation of the nanoparticles formulation and drug loading process is depicted in Fig. 1 together with a cartoon of the potential interaction established between thiolated micelles and mucus glycoproteins or in between polymeric chains to enhance particles stability.

2. Materials and methods

Materials. 11,1,4,7,10,10-Hexamethyltriethylenetetramine 97 % (HMTETA), 2-Hydroxyethil 2-bormoisobutyrate 95 % (OH-EBiB), 2-Hydroxyethylmethacrylate 97 % (HEMA), 2-Propanol ≥ 99.8 %, Acetonitrile (ACN), Aluminum oxide (Al_2O_3), N,N-dimethylformamide ≥ 99.8 % anhydrous (DMF), Tetrahydrofuran ≥ 99.9 % anhydrous inhibitor-free (THF), Tetrahydrofuran ≥ 99.9 % containing 250 ppm BHT as inhibitor (THF), Benzyl alcohol 99.8 % anhydrous (BnOH), α-Bromoisobutyryl bromide 98 % (BiBB), 2,2′-Bipyridyl ≥ 99 % (BPY), Copper (I) bromide 98 % (CuBr(I)), Copper (II) chloride 97 % ($CuCl_2$(II)), Deuterochloroform ≥ 99.8 % ($CDCl_3$), Dichloromethane ≥ 99.8 % (DCM), Diethyl ether ≥ 99.8 % (Et_2O), Ethyl-α-bromoisobutyrate 98 % (EBiB), ε-Caprolactone 97 % (ε-CL), Glycidyl methacrylate (gMA), L-Ascorbic acid 99 % (AA), Lithium bromide 99 % anhydrous (LiBr), Methanol ≥ 99.8 % (MeOH), N,N-Dimethylformamide ≥ 99.8 % (DMF), Poly (ethylene glycol) methyl ether methacrylate M_n = 500 Da (PEGMA), Doxorubicin hydrochloride (DOX), Sodium bicarbonate ($NaHCO_3$), Sodium Sulphate ≥ 99 % (Na_2SO_4), Sodium Chloride ≥ 99 % (NaCl), Tetrahydrofuran ≥ 99.9 % gel permeation chromatography grade (THF), Thioacetic acid 96 % (TAA), Tin(II) 2-ethylhexanoate 92–100 % ($Sn(Oct)_2$), Triethylamine ≥ 99 % (TEA), Toluene ≥ 99.9 % anhydrous, Mucin from porcine stomach (Type II, bound sialic acid, ≤1.2 %),Bovine Serum Albumin ≥ 97 % fatty acid free essentially globulin free (BSA), 5,5′-Dithio-bis-(2-nitrobenzoic Acid) ≥ 98 % (DTNB, Ellman's Reagent), Sodium phosphate ≥ 99 % (Na_2HPO_4), Tris (2-carboxyethyl)phosphine immobilized on Agarose CL-4B (TCEP), were all purchased from Sigma-Aldrich (Merck, Italy). Dimethyl Sulfoxyde-d_6 100 % (DMSO-d_6), Deuterium Oxide 100 % (D_2O) were purchased from Eurisotop (Cambridge Isotope Laboratories, France). N,N-Dimethylacetamide ≥ 99.5 % (DMAc) was purchased from ThermoFisher Scientific (Italy). Glycerol mono methacrylate (GMA) was purchased from Polysciences (Germany). Tris (2-pyridylmethyl) amine (TPMA) was purchased from Tokyo Chemical Industry (Belgium). All chemicals were used without further purification unless otherwise indicated. Deionized water (18.2 MΩ) was obtained from Millipore Milli-Q purification unit.

Polymers characterization. Monomer conversion (χ) and polymer degree of polymerization (DP) were determined by ^{1}H NMR analysis, dissolving crude and purified polymers in the proper deuterate solvent. ^{1}H NMR spectra were recorded on Bruker Avance 400 MHz and 500 MHz instruments at 298 K, using $CDCl_3$ or DMSO-d_6 as solvent. Chemical shifts (δ) are reported in ppm downfield from the deuterated solvent used as internal standard, and the coupling constants (J) are expressed in Hz.

The polymers number-average molar mass ($M_{n,SEC}$) and dispersity (Đ = M_w/M_n) values were evaluated using two different Jasco® LC-2000Plus size exclusion chromatography (SEC) instruments both equipped with a refractive index detector (RI-2031Plus, Jasco), a CO-2060 plus oven column, and a PU-2080 pump. The first SEC system employs three Agilent PL Cgel columns, 300 × 7.5 mm (MW range: 5 × 10^2 to 17 × 10^5 g/mol), 5 μm particle size (10E4, 10E5, 500 A) and a PLC gel guard 50 × 7.5 mm, 5 μm particle size, using THF as eluent at 35 °C. The second SEC system works with three GRAM columns, 300 × 8 mm, 10 μm particle size (1000, 100, 30 A), and a GRAM guard, 50 × 8 mm, 10 μm particle size, using DMAc (30 mM LiBr) as eluent at 40 °C. Both the machineries were calibrated by using polystyrene standards (calibration kits by RESTEK and Sigma-Fluka). According to the compounds solubility, samples of purified polymer were dissolved in THF (containing 250 ppm BHT as inhibitor) or DMAc at a concentration of 4 mg/mL, filtered through PTFE syringe filters (0.22 μm) and injected at a flow rate of 1 mL/min, using a Jasco AS-2055Plus autosampler.

Synthesis of PCL_n. The monomer (M) ε-caprolactone (5 g, 43.8 mmol), was inserted in a round double neck flask and three cycles of nitrogen/vacuum of 5 min each were performed. The initiator (I) BnOH (eq. M/eq. I=n, where n = 20, 30, 40, 50)) and the catalyst (C) $Sn(Oct)_2$ (eq. C/eq. I=0.1) were then added, maintaining the system under N_2 flow. The mixture was stirred overnight at 130 °C. The reaction was stopped by cooling the flask to room temperature. Purification was carried out by dissolving the crude in DCM (2.5 g/mL) and dropping it into cold MeOH (MeOH/DCM=100/1 v/v). The system was kept under vigorous stirring in an ice bath throughout the precipitation process. The resulting precipitate was isolated from the supernatant through filtration, and the filtrate was dried under reduced pressure at 50 °C, obtaining the final product as a white powder. Yield > 90 %. Conversion χ = 99 % (from ^{1}H NMR data). ^{1}H NMR (400 MHz, $CDCl_3$), δ (ppm): δ 7.34–7.32 (s, 5H, C_6H_5-CH_2-), 5.11–5.09 (s, 2H, C_6H_5-CH_2-OC(O)-), 4.06–4.03 (t, 2H·(*n*-1), –CH_2-OC(O)-), 3.64–3.61 (t, 2H, –CH_2-OH), 2.30–2.28 (t, 2H·*n*, –OC(O)–CH_2-), 1.64 (m, 4H·*n*, –OC(O)–CH_2CH_2-, –CH_2CH_2-OC(O)-), 1.38–1.36 (m, 2H·*n*, –$CH_2CH_2CH_2$-), where *n* is PCL degree of polymerization.

Synthesis of PCL_n-Br. 5 g of PCL_n (1 eq.) were added in a two-neck flask then evacuated and backfilled with nitrogen three times, dissolved in 6 mL of dry toluene, and cooled at 0 °C in an ice bath. TEA (1.7 eq.) and BiBB (1.5 eq.) were dissolved in 1 mL of toluene each and stirred for 10 min. TEA and BiBB solutions were added dropwise to the reaction mixture through a dropping funnel. The reaction mixture was then brought back to r.t. And stirred overnight at 60 °C in an oil bath. The resulting solution was dried under reduced pressure until toluene complete evaporation, and the crude product was dissolved in 5 mL of DCM. The solution was the filtered to remove the salts formed during the reaction, washing the glassware and the paper filter used with 10 additional mL of DCM to avoid product losses. An aqueous solution (φ_{acq}) of $NaHCO_3$ at pH≥8 was prepared dissolving ~ 3 g of salt in 60 mL of water. The polymer solution (φ_{org}) obtained after the filtration was inserted in a separating funnel and washed three times with the $NaHCO_3$ solution ($\varphi_{org}/\varphi_{acq}$ ~ 1/1 v/v for each wash) to extract the desired product in the organic phase. The water phase collected at the end of the washing steps was mixed with additional DCM ($\varphi_{org}/\varphi_{acq}$ ~ 1/1 v/v) for the complete recovery of the product. Anhydrous Na_2SO_4 was added to

the organic solution for water adsorption, with consequent salt removal through filtration. The filtrate was dried under reduced pressure, then dissolved in 2 mL of DCM and dropped in 250 mL of cold MeOH, maintaining the system under stirring in an ice bath. The solution was then filtered to isolate the precipitate, obtaining the final product as a slightly yellow viscous oil. Yield > 90 %. Conversion $\chi = 100$ % (from ^{1}H NMR data). ^{1}H NMR (400 MHz, $CDCl_3$), δ (ppm): δ 7.34 (m, 5H, C_6H_5-CH_2-), 5.11 (s, 2H, C_6H_5-CH_2-OC(O)-), 4.06–4.05 (t, 2H·*n*, –CH_2-OC(O)-), 2.30 (t, 2H·*n*, –OC(O)–CH_2-), 1.93–1.92 (s, 6H, –$C(CH_3)_2$Br), 1.65 (m, 4H·*n*, –OC(O)–CH_2CH_2-, –CH_2CH_2-OC(O)-), 1.38 (m, 2H·*n*, –$CH_2CH_2CH_2$-), where *n* is PCL degree of polymerization

Synthesis of PCL_n-b-[$P(PEGMA)_q$-co-$PgMA_m$]. THF (inhibitor free) was degassed under nitrogen for 30 min. The reaction macroinitiator (I) PCL_n-Br (500 mg, 1 eq.) and the monomers PEGMA and gMA were added to a Schlenk flask and three cycles of nitrogen/vacuum of 5 min each were performed. The monomers amount was calculated according to the target degree of polymerization (eq. PEGMA/eq. I=q, eq. gMA/eq. I=m, where q = 5, 10, 15, 20, 25, 30, 35 and m = 0, 1, 2, 3). The catalyst solution (C) was prepared as follows: Cu(I)Br (574 mg) was inserted in a double neck flask, and three cycles vacuum/nitrogen were performed. Degassed THF (5 mL) and the ligand (L) HMTETA (1 mL) were added, obtaining a mixture that was stirred at r.t. under N_2 for 10 min·THF was added to the reaction mixture ([PEGMA] ≤ 1 M), and the flask was heated and kept at 50 °C until complete dissolution of the solid components. Finally, the required amount of catalyst solution ([C]/[L]/[I] = 1/1/1) was added to the monomers. The reaction mixture was stirred overnight at 50 °C. The purification was performed by filtering the reaction mixture through a neutral alumina pad (h = 3 cm, Φ = 2 cm), washing with THF. Then the filtrate was dried under reduced pressure and the resulting crude was dissolved in DCM (2 mg/mL) and dropped in cold Et_2O (DCM/Et_2O=1/100 v/v), maintaining the system under stirring in ice bath. The mixture was stored at − 20 °C for 30 min and the resulting precipitate was isolated by removing the supernatant through filtration. Yield 70–80 %. ^{1}H NMR (400 MHz, $CDCl_3$), δ (ppm): δ 7.34 (s, 5H, PCL: C_6H_5-CH_2-), 5.11 (s, 2H, PCL: C_6H_5-CH_2-OC(O)-), 4.3–3.8 (s, 2H·*m*, gMA: −O-CH_2-CH-), 4.14–4.02 (m, 2H·*n* + 4H, PCL: –CH_2-OC(O)-, PEG: −O-CH_2CH_2-O-), 3.6 (m, 4H·8·*q*, PEG: –CH_2CH_2-), 3.38 (s, 3H·*q*, PEG: –OCH_3), 3.2 (s, 1H·*m*, gMA: –CH_2-CH-), 2.8–2.6 (d, 2H·*m*, gMA: –CH-CH_2-O-), 2.32–2.25 (t, 2H·*n*, PCL: –OC(O)–CH_2-), 1.92 (s, 6H, –CH_2OC(O)C(CH_3)$_2$-), 1.48–1.65 (m, 4H·*n*, PCL: –OC(O)–CH_2CH_2-, –CH_2CH_2-OC(O)-), 1.25–1.38 (m, 2H·*n*, PCL: –$CH_2CH_2CH_2$-), 1.2–0.6 (m, 3H·(*m* + *q*), PEG: $CH_{3,backbone}$, gMA: $CH_{3,backbone}$), where *n* is PCL degree of polymerization, *m* is PgMA degree of polymerization, *q* is P(PEGMA) degree of polymerization.

Synthesis of PCL_n-b-$PgMA_m$. THF (inhibitor free) was degassed under nitrogen for 30 min. The reaction macroinitiator (I) PCL_n-Br (500 mg, 1 eq.) and the desired amount of monomer gMA (eq. gMA/eq. I=m) were added to a Schlenk flask and three cycles of nitrogen/vacuum of 5 min each were performed. The catalyst-ligand solution (C-L) was prepared as it follows: Cu(I)Br (574 mg) and BPY (1249 mg) were inserted in a double neck flask, and three cycles vacuum/nitrogen were performed. Degassed THF (5 mL) was added, obtaining a green mixture that was stirred at r.t. under N_2 for 10 min·THF was added to the reaction mixture ([gMA] ≤ 1 M), and the flask was heated up to 50 °C, until complete dissolution of the solid component. Finally, the required amount of catalyst solution ([C]/[L]/[I] = 1/2/1) was added to the monomers. The reaction mixture was stirred overnight at 50 °C. The purification was performed by filtering the reaction mixture through a neutral alumina pad (h = 3 cm, Φ = 2 cm), washing with THF. The filtrate was dried under reduced pressure and the resulting crude was dissolved in DCM (2 mg/mL) and dropped in cold Et_2O (DCM/Et_2O=1/100 v/v), maintaining the system under stirring in an ice bath. The mixture was stored at − 20 °C for 30 min and the resulting precipitate was isolated by removing the supernatant through filtration. Yield 90 %. ^{1}H NMR (400 MHz, $CDCl_3$), δ (ppm): δ 7.34 (s, 5H, PCL: C_6H_5-CH_2-), 5.11 (s, 2H, PCL: C_6H_5-CH_2-OC(O)-), 4.3–3.8 (s, 2H·*m*, gMA: −O-CH_2-CH-), 4.14–4.02 (m, 2H·*n*, PCL: –CH_2-OC(O)-), 3.2 (s, 1H·*m*, gMA: –CH_2-CH-), 2.8–2.6 (d, 2H·*m*, gMA: –CH-CH_2-O-), 2.32–2.25 (t, 2H·*n*, PCL: –OC(O)–CH_2-), 1.92 (s, 6H, –CH_2OC(O)C(CH_3)$_2$-), 1.48–1.65 (m, 4H·*n*, PCL: –OC(O)–CH_2CH_2-, –CH_2CH_2-OC(O)-), 1.25–1.38 (m, 2H·*n*, PCL: –$CH_2CH_2CH_2$-), 1.2–0.6 (m, 3H·(*m* + *q*), gMA: $CH_{3,backbone}$), where *n* is PCL degree of polymerization, *m* is PgMA degree of polymerization, *q* is PGMA degree of polymerization.

Synthesis of PCL_rMA. The monomer (M) ε-CL (5 g, 43.8 mmol, r eq.) was inserted in a round double neck flask and three cycles of nitrogen/vacuum of 5 min each were performed. A solution containing the initiator (I) HEMA (eq. M/eq. I=n) and the catalyst (C) $Sn(Oct)_2$ (eq. C/eq. I=0.1) was prepared, stirred under a N_2 flow for 10 min, and then added to the monomer, maintaining the system under N_2 flow. The mixture was stirred overnight at 130 °C. The reaction was stopped by cooling the flask to room temperature. Purification was carried out by dissolving the crude in DCM (2.5 g/mL) and dropping it in cold water (water/DCM=100/1 v/v). The system was kept under vigorous stirring and in an ice bath for the precipitation process. The resulting precipitate was isolated from the supernatant through filtration, redissolved in DCM and anhydrified with anhydrous Na_2SO_4. Subsequently it was filtered, and the filtrate was dried under reduced pressure, obtaining a colorless viscous oil. Yield > 90 %. Conversion $\chi = 99$ % (from ^{1}H NMR data). ^{1}H NMR (400 MHz, $CDCl_3$), δ (ppm): 6.11 (s, 1H, H_2C-C(CH_3)-), 5.58 (s, 1H, H_2C-C(CH_3)-), 4.37–4.28 (m, 4H, –OCH_2CH_2O-), 4.05 (t, 2H·(*r*-1), –CH_2-OC(O)-), 3.63 (t, 2H, –CH_2-OH), 2.29 (m, 2H·*r*, –OC(O)–CH_2-), 1.94 (s, 3H, H_2C-C(CH_3)-), 1.69–1.58 (m, 4H·*r*, –OC(O)–CH_2CH_2-, –CH_2CH_2-OC(O)-), 1.44–1.32 (m, 2H·*r*, –$CH_2CH_2CH_2$-), where *r* is PCL degree of polymerization.

Synthesis of $[PCL_r]_n$. THF (inhibitor free) was degassed under nitrogen flow for 30 min. The catalyst-ligand solution was prepared as follow: the catalyst (C) CuBr (143.5 mg) was inserted in a Schlenk tube

and three cycles of nitrogen/vacuum of 5 min each were performed. The ligand (L) HMTETA (0.27 mL) and degassed THF (5 mL) were added, obtaining a dark green mixture that was stirred at r.t. under nitrogen flow for 10 min. Macromonomer PCL_rMA (5 g, n eq.) was inserted in a two-neck flask then evacuated and backfilled with nitrogen three times, dissolved in THF ($[PCL_rMA] = 1$ M) and heated to 50 °C. The required amount of catalyst-ligand solution and of the initiator (I) EBiB ([C]/[L]/[I] = 1/1/1) were then added to the monomer. The reaction mixture was stirred overnight at 60 °C. The purification was performed filtering the reaction mixture through a neutral alumina pad (h = 3 cm, Φ = 2 cm), washing with THF. The product obtained was dried under reduced pressure and the resulting crude was dissolved in DCM (2 g/mL). It was subsequently dropped in cold Et_2O (Et_2O/DCM=100/1 v/v) maintaining the system under stirring in an ice bath. The mixture was stored at −20 °C for 30 min and the resulting precipitate was isolated by removing the supernatant through filtration. Yield > 95 %. ^{1}H NMR (400 MHz, $CDCl_3$), δ (ppm): *δ* 4.40–4.10 (m, 4H, –C*H*$_2$C*H*$_2$-OC(O)-backbone-), 4.05 (t, 2H·(*r*-1), –C*H*$_2$-OC(O)-), 3.64 (t, 2H, –C*H*$_2$OH), 2.40–2.24 (m, 2H·*r*, –OC(O)–C*H*$_2$-), 2.04–1.72 (m, 2H, –C*H*$_{2,backbone}$-), 1.72–1.52 (m, 4H·*r*, –OC(O)–CH$_2$C*H*$_2$-, –C*H*$_2$CH$_2$-OC(O)-), 1.45–1.31 (m, 2H, –CH$_2$C*H*$_2$CH$_2$-), 1.07–0.59 (m, 3H, –C*H*$_{3,backbone}$), where *r* is the PCL degree of polymerization.

Synthesis of $[PCL_r\text{-}Br]_n$. 5 g of $[PCL_r]_n$ (1 eq.) were added to a two-neck flask. This was evacuated and backfilled with nitrogen three times, dissolved in 6 mL of dry toluene, and cooled at 0 °C in an ice bath. TEA (1.7 · n eq.) and BiBB (1.5 · n eq.) were dissolved in 2 mL of dry toluene each and stirred for 10 min. TEA and BiBB solutions were added dropwise to the reaction mixture through a dropping funnel; 4 additional mL of toluene were used to wash both the glass vial in which the reagents were dissolved and the funnel. The reaction mixture was then brought back to r.t. And stirred overnight at 60 °C in an oil bath. The resulting solution was dried under reduced pressure and the crude obtained was dissolved in 5 mL of DCM. The solution was the filtered to remove the salts formed during the reaction, washing the glassware and the paper filter with additional 10 mL of DCM to avoid product losses. An aqueous solution (φ_{acq}) of $NaHCO_3$ at pH≥8 was prepared dissolving ~ 3 g of salt in 60 mL of water. The polymer solution (φ_{org}) obtained after the filtration was inserted in a separating funnel and washed three times with the $NaHCO_3$ solution ($\varphi_{org}/\varphi_{acq}$ ~ 1/1 v/v for each wash) to extract the desired product in the organic phase. The water phase collected at the end of the washing steps was mixed with additional DCM ($\varphi_{org}/\varphi_{acq}$ ~ 1/1 v/v) for the complete recovery of the product. Anhydrous Na_2SO_4 was added to anhydrify the organic solution with consequent salts removal through filtration. The filtrate was dried under reduced pressure, dissolved in 2 mL of DCM, and dropped in 250 mL of cold MeOH, maintaining the system under stirring in an ice bath. The solution was stored in the freezer at − 20 °C and filtered to isolate the precipitate, obtaining the final product as a slightly yellow viscous oil. Conversion χ = 100 % (from ^{1}H NMR data). Yield > 90 %. ^{1}H NMR (400 MHz, $CDCl_3$), δ (ppm): *δ* 4.45–4.10 (m, 6H, –C*H*$_2$C*H*$_2$-OC(O)-backbone-, –C*H*$_2$OC(O)C(CH$_3$)$_2$Br), 4.06 (t, 2H·(*r*-1), –C*H*$_2$-OC(O)-), 2.40–2.24 (m, 2H·*r*, –OC(O)–C*H*$_2$-), 1.93 (s, 6H, − C(C*H*$_3$)$_2$Br), 1.76–1.59 (m, 4H·*r*, –OC(O)–CH$_2$C*H*$_2$-, –C*H*$_2$CH$_2$-OC(O)-), 1.48–1.30 (m, 2H, –CH$_2$C*H*$_2$CH$_2$-), 1.07–0.70 (m, 3H, –C*H*$_{3,backbone}$), where *r* is PCL degree of polymerization

Synthesis of $[PCL_r\text{-}b\text{-}[P(PEGMA)_q\text{-}co\text{-}PgMA_m]]_n$. THF (inhibitor free) was degassed under nitrogen for 30 min. The reaction macroinitiator (I) $[PCL_r\text{-}Br]_n$ (500 mg, 1 eq.) and the monomers PEGMA and gMA were added to a Schlenk flask and three cycles of nitrogen/vacuum of 5 min each were performed. The monomers amount was calculated according to the target degree of polymerization, considering each chain (n) of the macromonomer $[PCL_r\text{-}Br]_n$ as an initiator (eq. PEGMA/eq. I=q · n, eq. gMA/eq. I=m × n, where q = 5, 10, 15, 20, 25, 30 and m = 0, 1, 2, 3). The catalyst-ligand solution was prepared as it follows: Cu(I)Br (C) (574 mg) was inserted in a double neck flask, and three cycles vacuum/nitrogen were performed. Degassed THF (5 mL) and the ligand (L) HMTETA (1 mL) were added, obtaining a green mixture that was stirred at r.t. under N_2 for 10 min·THF was added to the reaction mixture ([PEGMA] ≤ 0.1 M), and the flask was heated up to 50 °C, until complete dissolution of the solid components. Finally, the required amount of catalyst solution ([C]/[L]/[I] = 1 · n/1 · n/1) was added to the monomers. The reaction mixture was stirred overnight at 50 °C. The purification was performed by filtering the reaction mixture through a neutral alumina pad (h = 3 cm, Φ = 2 cm), washing with THF. Then the filtrate was dried under reduced pressure and the resulting crude was dissolved in DCM (2 mg/mL) and dropped in cold Et_2O (DCM/Et_2O=1/100 v/v), maintaining the system under stirring in an ice bath. The mixture was stored at − 20 °C for 30 min and the resulting precipitate was isolated by removing the supernatant through filtration. Yield 60–80 %. ^{1}H NMR (400 MHz, $CDCl_3$), δ (ppm): *δ* 4.27–3.81 (s, 2H·m, gMA: −C(O)-O-CH$_2$-CH-), 4.12–3.99 (m, 4H+2H·*r*, PCL: –OC(O)C*H*$_2$C*H*$_2$OC(O)-backbone-, –C*H*$_2$-OC(O)-), 3.73–3.50 (m, 4H·*8*·*q*, PEG: –C*H*$_2$C*H*$_2$-), 3.37 (s, 3H·*q*, PEG: –OC*H*$_3$), 3.19 (s, 1H·m, gMA: –CH$_2$-CH(O)–CH$_2$-), 2.83–2.62 (s, 2H·m, gMA: –CH-CH$_2$-O-), 2.36–2.23 (m, 2H·*r*, PCL: –OC(O)–C*H*$_2$-), 1.92 (s, 6H, –CH$_2$OC(O)C(C*H*$_3$)$_2$-), 1.71–1.55 (m, 4H·*r*, PCL: –OC(O)–CH$_2$C*H*$_2$-, –C*H*$_2$CH$_2$-OC(O)-), 1.44–1.31 (m, 2H·*r*, PCL: –CH$_2$C*H*$_2$CH$_2$-), 1.14–0.67 (m, 3H·(*m* + *q*), PEG: CH$_{3,backbone}$, gMA: CH$_{3,backbone}$), where *r* is PCL degree of polymerization, *m* is PgMA degree of polymerization, *q* is P(PEGMA) degree of polymerization.

Post functionalization with thioacetic acid. THF (inhibitor free) was degassed under nitrogen for 30 min. 500 mg of copolymer containing the reactive glycidyl units was inserted in a Schlenk flask and three cycles of nitrogen/vacuum were performed. Degassed THF (5 mL) was added to the copolymer, and it was stirred under nitrogen flux until complete dissolution. Thioacetic acid (TAA) and TEA where then added to the reaction mixture (eq. epoxy ring/eq. TAA/eq. TEA=1/1/3) maintaining the system under nitrogen flux. The solution was stirred overnight at 25 °C. The mixture obtained was dried under reduced pressure and the resulting crude was dissolved in 15 mL of DCM (φ_{org}). An aqueous solution saturated with NaCl (φ_{acq}) was prepared. The polymer solution φ_{org} was inserted in a separating funnel and washed three times with the NaCl solution ($\varphi_{org}/\varphi_{acq}$ ~ 4/1 v/v for each wash) to extract the desired product in the organic phase. The water phase collected at the end of the washing steps was mixed with additional DCM for the complete recovery of the product. Anhydrous Na_2SO_4 was added to anhydrify the organic solution with consequent salts removal through filtration. The filtrate was dried under reduced pressure, dissolved in 2 mL of DCM, and dropped in 250 mL of hexane, maintaining the system under stirring. Conversion χ = 100 % (from ^{1}H NMR data). Yield > 80 %. ^{1}H NMR (400 MHz, DMSO-d_6), δ (ppm): *δ* 7.34 (s, 5H, PCL: C$_6$H$_5$-CH$_2$-), 5.11 (s, 2H, PCL: C$_6$H$_5$-CH$_2$-OC(O)-), 5.29 (s, 1H·*m*, gMA: OH-CH–), 4.10–3.90 (m, 2H·*n* + 4H·*q* + 3H·*m*, PCL: –CH*2*-OC(O)-, PEG: −O-CH$_2$CH$_2$-O-, gMA: −O-CH$_2$-CH), 3.5 (m, 4H·8·*q*, PEG: –CH$_2$CH$_2$-), 3.38 (s, 3H·*q*, PEG: –OCH$_3$), 3.25 (s, 1H·*m*, gMA: –CH$_2$-CH–), 2.32–2.25 (t, 2H·*n*, PCL: –OC(O)–CH$_2$-), 2.08 (s, 3H·*m*, gMA: −S(O)–CH$_3$), 1.60–1.49 (m, 4H·*n*, PCL: –OC(O)–CH$_2$CH$_2$-, –CH$_2$CH$_2$-OC(O)-), 1.35–1.22 (m, 2H·*n*, PCL: –CH$_2$CH$_2$CH$_2$-), 1.05–0.6 (m, 3H·(*m* + *q*), PEG: CH$_3$,backbone, gMA: CH$_3$,backbone), where n is PCL degree of polymerization, m is PgMA degree of polymerization, q is P(PEGMA) degree of polymerization

Nanoparticles formulation. Nanoparticles (NPs) were prepared according to a nanoprecipitation/solvent evaporation method [25,35,60]. Briefly, from 10 to 20 mg of copolymer were dissolved under stirring in 1 mL of acetone. The solution was added dropwise into 1 mL of PBS (10 mM, pH 7.4) or ultrapure water and stirred for 10 min. Acetone was removed at the rotary evaporator under controlled gradient of pressure (from 1000 mbar to 100 mbar in 1 h and then 1 h at 100 mbar) at 32 °C. An aliquot of 700 μL was withdrawn from each nanoparticles batch and filtered (through PTFE syringe filters (0.45 μm) for characterization. Particle size distribution, average size (Z-Av.), and polydispersity index (PdI) of the nanoparticles in suspension (1 mg/mL in PBS 10 mM, pH 7.4) at 25 °C were evaluated via Dynamic Light

Scattering (DLS) using a Malvern Zetasizer Nano ZS, equipped with a 4 mW He − Ne laser operating at λ = 634 nm (backscattered angle 173°). While, for Transmission electron microscopy (TEM) analysis, a volume of 10 μL of nanoparticle suspension in ultrapure water (5 mg/mL) were dropped on Lacey carbon coated copper TEM grids (400 mesh) or on copper TEM grid (400 mesh, no carbon film). The grid was left to dry overnight to evaporate the solvent. Images of the nanocarriers suspension were acquired on a CM200FEG Philips microscope. The acquisitions were performed at 200 kV and processed for particles size evaluation using ImageJ software.

Drug loading. 1 mg of Doxorubicin hydrochloride (DOX-HCl) was dissolved in 0.5 mL of ultrapure water, and then added dropwise into 1 mL of polymer suspension (10 mg/mL) in PBS (10 mM, pH 7.4). The mixture was stirred overnight at 35 °C to induce DOX encapsulation given the enhanced hydrophobicity of the dimerized formed obtained at physiological pH [77]. The unloaded DOX was removed by ultrafiltration with Centrifugal filters (Amicon, MWCO 10 kDa) at 2500 rcf for 10 min, washing four times with 1 mL of PBS to obtain 1.5 mL of DOX-loaded nanoparticles. The amount of DOX encapsulated in the polymeric nanocarriers was determined by using a Jasco FP-8500 spectrofluorometer, equipped with a 150 w Xe lamp as the excitation source. The fluorescence intensity was measured by setting $\lambda_{ex}/\lambda_{em}$ = 480/555 nm, for DOX solutions in PBS buffer pH 7.4. The amount [mg] of DOX encapsulated in the NPs was assessed by means of a calibration curve that correlated the measured fluorescence intensity to the amount of DOX in PBS (Figure S1, Supporting Information). The fluorescence of the polymeric micelles and of the buffer alone were also measured, giving fluorescent intensity < 10 [a.u] which is negligible with respect to the ones detected at different DOX concentrations

Drug loading (DL) and encapsulation efficiency (EE) were calculated according to *Equation (1)*.

$$DL = \frac{DOX\ loaded\ weight\ [mg]}{Solid\ phase\ weight\ [mg]}\%$$

$$EE = \frac{DOX\ loaded\ weight\ [mg]}{DOX\ feed\ weight\ [mg]}\% \quad (1)$$

The fluorescence analysis was performed withdrawing 200 μL of the DOX-loaded NPs suspension while an additional aliquot of 700 μL of DOX-loaded NPs was analyzed at DLS for a comparison of the particles size distribution and average size with the ones obtained before DOX loading.

Thiols deprotection and particle size reduction assessment. Copolymers functionalized with thioacetic acid were employed to obtain 1 mL of NP suspension (20 mg/mL) in MilliQ water. Thiols deprotection was carried out with a basic-catalyzed hydrolysis reaction at 25 °C adding NaOH aqueous solution to the NPs suspension to reach a final pH=9. To assess the reaction kinetic, two aliquots from the reaction mixture (250 μL) were withdrawn at different time points (5, 10, 20, 30, 45, 60, 75 min) to be processed according to the Ellman's Reagent (DTNB) assay procedure [61,78,79] for quantitating sulfhydryl groups based on molar absorptivity (ThermoScientific, Instructions Ellman's Reagent, 22582).

The number of moles of free sulfhydryl groups was evaluated correlating the absorbance of each sample (*A*), with the sulfhydryl molar concentration (*c*), by means of the known TNB molar absorptivity (*E*, molar extinction coefficient). The absorbance measurements were performed at 25 °C, on a Jasco V-630 UV–vis spectrophotometer set at 412 nm and using 1 cm (*b,* path length) PPMA disposable cuvettes. In the system considered and at the fixed wavelength, TNB molar extinction coefficient is defined as reported in *Equation (2)*.

$$E = \frac{A}{bc} = 14150\ \frac{1}{cm\,M} \quad (2)$$

For each sampling, one of the two aliquots withdrawn was formerly treated with an immobilized TCEP disulfide reducing agarose gel following the general procedure for reduction in batch format (for 20—–750 μL samples)(ThermoScientific, Instructions Immobilized TCEP Disulfide Reducing Gel, 77712). The actual number of free −SH groups present in the polymer formulation was calculated, taking into account the dilution factors arising from the dilution of the collected reaction mixture aliquots to bring the pH of the suspension back to a physiological value, and from Ellman's sample preparation using Ellman's reagent buffer. To determine NP size variation after thiols deprotection, DLS measurements were performed before the hydrolysis and at different time points after complete thiols deprotection by resuspending the NPs in PBS 10 mM to reach a pH=7.4.

Mucin and protein adhesion assay. The adhesion of thiolated polymers on mucins and proteins was tested by preparing solutions of mucin from porcine stomach (1 mg/mL), BSA (10 mg/mL), thiolated polymers (2 mg/mL) and non-thiolated polymers (as negative control, 2 mg/mL) in PBS 10 mM pH 7.4 [75,80]. The same amount of biomaterials and buffer volumes were used to formulate polymers-mucin and polymers-BSA mixtures. Polymers functionalized with TAA underwent a deprotection reaction (as described in the section above), to obtain a certain percentage of free −SH groups, according to their initial degree of functionalization with glycidyl units. The resulting thiolated polymers and non-thiolated polymers suspensions were mixed with a micropipette for 10 s with mucin or BSA (previously dissolved in PBS), and aliquots of 700 μL were withdrawn to be analyzed. The detection of aggregate formations was performed via DLS analysis (Malvern Zetasizer Nano ZS, 4 mW He − Ne laser, λ = 634 nm, backscattered angle 173°), measuring the differences in the scattered intensity (kpcs) (derived count rate), size distribution and average size (Z-Av.) between the single component suspensions and the ones of their relative mixtures. Simultaneously, variation of optical density (O.D.) of the same samples were measured via UV–Vis analysis at 420 nm (Jasco-630 UV–vis spectrophotometer, 25 °C, 1 cm path length disposable cuvettes). The testing was performed right after the mixtures formulation, 1 h and 2 h later to determine possible modification in time of the parameters examined.

3. Results and discussion

3.1. Polymer design and characterization

A library of amphiphilic macromolecules of complex topology was obtained via a combination of ROP and ATRP. These controlled-living polymerizations were employed in a stepwise fashion, depending on the targeted macromolecular architecture, to synthesize P(PEGMA) or PGMA based copolymers, combined with the functionalizable PgMA, and PCL as hydrophobic block (Fig. 2).

The PCL blocks were firstly obtained via a bulk ROP of ε-CL monomer. In order to produce series of linear or brush block copolymers, two synthesis strategies were adopted, according to the desired topology. A linear PCL was synthesized using BnOH as initiator and $Sn(Oct)_2$ as catalyst [1], whereas, to produce a comb-like polyester, the same ROP reaction was performed using HEMA as initiator to obtain PCL_rMA macromonomers. In this case, a further polymerization step was required to obtain $[PCL_rMA]_n$ from EBiB. This ATRP was conducted in THF, employing CuBr as catalyst and HMTETA as ligand [1,25,60]. Polyester blocks with predetermined degree of polymerization (DP) and molecular weight were obtained with a monomer conversion (χ_{CL}, calculated via ^{1}H NMR analysis) for ε-CL ROP above 98 % for all the synthesis performed, regardless the initiator used. In both linear and comb-like structures, the terminal –OH groups of the PCL chains were additionally functionalized with an isobutyryl bromide moiety (100 % conversion), to serve as ATRP macroinitiators for the subsequent synthesis of the hydrophilic block. Starting from these hydrophobic macrostructures, successive ATRP were carried out to achieve the final amphiphilic macromolecules of different architecture, composition, and degree of functionalization. The polymer series produced were named

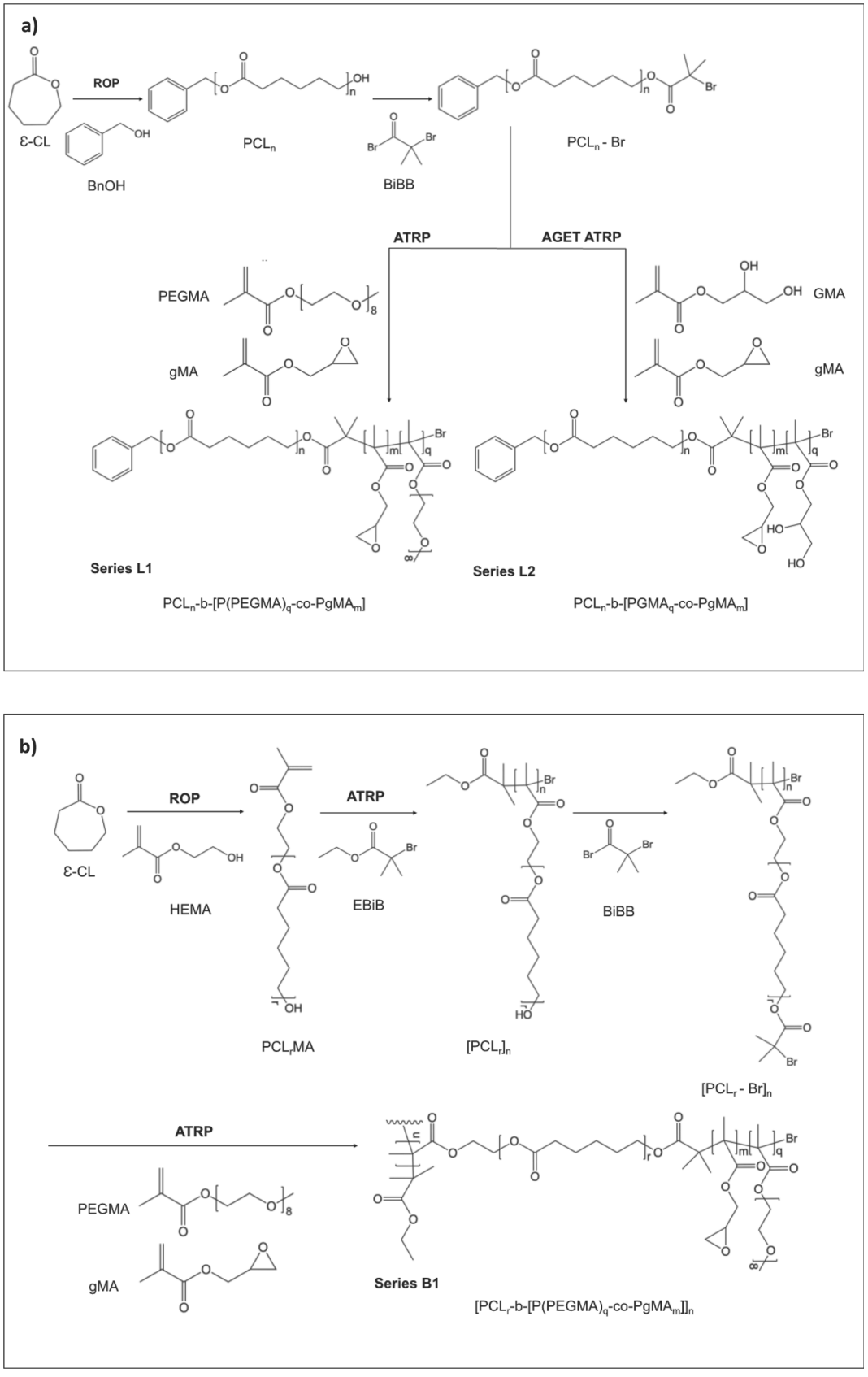

Fig. 2. Synthetic pathway and nomenclature of Series L1 and L2 (linear copolymers) **(a)**, and Series B1 (brush block copolymers) **(b)**.

Series L1, Series L2 and Series B1 based on their architecture (linear (L) or branched (B)) and main hydrophilic constituents (PEGMA (1) or GMA (2)).

Series L1 consists in linear block copolymers with general formula PCL_n-b-[$P(PEGMA)_q$-co-$PgMA_m$]. They were synthesized through ATRP by randomly copolymerizing different percentages of commercially available PEGMA macromonomer (average M_n = 500 Da, with 8/9 ethylene oxide repeating units) and gMA, in presence of Cu(I)Br/HMTETA catalyst [1,25,60,81], and using PCL_n-Br as macroinitiator in THF. Alternatively, Series L2 copolymers, with general formula PCL_n-b-[$PGMA_q$-co-$PgMA_m$], were obtained by random copolymerization of different ratios of GMA and gMA monomers. Also this case, linear PCL_n-Br was also employed as macroinitiator, but an AGET ATRP was required for achieving controlled character, using $CuCl_2$ and TPMA as catalyst, ascorbic acid as reducing agent, and DMF as solvent.

For both Series L1 and L2, a DP of 30 units was initially targeted for the polyester chain (n = 30), which finally constitute the inner core of the self-assembled NPs. The length of the hydrophilic portion (m + q) was varied from 5 to 35/40 units to study how the hydrophilic/hydrophobic molar ratio may affect the amphiphilic properties of the polymers and their self-assembly behavior in water. Regarding the two series of linear block copolymers considered, two different hydrophilic monomers (PEGMA and GMA) were used to understand if a shorter monomeric unit with less steric hindrance (such as GMA) may confer different features to the final nanoparticles compared to PEGMA.

In Series L1, copolymers with a fixed DP of PEGMA-co-gMA (m + q = 20) were also produced by varying the DP of polyester block from 20 to 50 units (n = 20, 30, 40, 50), aiming to evaluate the effect of the length of the PCL block on the physicochemical properties of the final macromolecules and on their interactions with the encapsulated drug.

For both PEGMA and GMA monomers, ATRP always achieved high conversions ($\chi \geq 85$ % after 6 h), as calculated from ^{1}H NMR spectroscopy. The reaction kinetic profiles were evaluated via ^{1}H NMR analysis to verify the linearity of the data obtained (expected for a first order kinetics), indicating an ongoing controlled polymerization (*Figure S2.a*, *Supporting Information*). SEC analysis confirmed a linear growth of the polymer average molecular weight (M_n) over monomer conversion, with a relatively narrow dispersity ($Đ \leq 1.3$) (*Figure S2.b*, *Supporting Information*), thus confirming the feasibility to obtain macromolecules with the predetermined DP (Table 1).

Regarding Series B1, the same random copolymerization of PEGMA and gMA adopted for Series L1 was employed to obtain macromolecules of general formula [PCL_r-b-[$P(PEGMA)_q$-co-$PgMA_m$]]$_n$. A [PCL_r-Br]$_n$ macroinitiator was chosen to design a bottlebrush containing an inner PCL domain and an outer hydrophilic domain composed of comb-like P(PEGMA-co-gMA). The aim was to investigate how a brush block architecture could provide different physicochemical characteristics to the resulting self-assembled NPs from the linear counterpart. The DP (n) of the comb-like PCL macroinitiator was set to 30, while the DP of each PCL pendant chains (r) was fixed at 15.

In order to conduct a parallel study with respect to linear copolymers, the length of the hydrophilic portion was also varied from 5 to 25 units to study how the hydrophilic/hydrophobic molar ratio affect self-assembly in water and the final NPs size. The PEGMA-co-gMA polymerizations confirmed high conversions ($\chi \geq 86$ % after 6 h from ^{1}H NMR spectroscopy) and good control over the molecular weight distribution (Table 1).

Glycidyl methacrylate units were statistically inserted within the hydrophilic constituent of the three series of polymers because of its reactive epoxy ring, which could be functionalized with different moieties, depending on the specific application. With the introduction of the copolymerization of PEGMA and GMA monomers with gMA, the polymerization reactions optimized in previous work were further refined. This included avoiding temperatures above 60 °C while minimizing monomer concentrations, in order to prevent premature opening of the epoxy ring and to avoid possible crosslinking of the reactive system. In

Table 1
Summary of properties of PCL_n-b-[$P(PEGMA)_q$-co-$PgMA_m$], PCL_n-b-[$PGMA_q$-co-$PgMA_m$] and [PCL_r-b-[$P(PEGMA)_q$-co-$PgMA_m$]]$_n$ copolymers. Conversion of PEGMA-co-gMA or GMA-co-gMA monomers by ATRP ($\chi_{PEGMA\text{-}gMA}$ or $\chi_{GMA\text{-}gMA}$), number average molecular weight ($M_{n,\ NMR}$) obtained by ^{1}H NMR and SEC ($M_{n,\ SEC}$) respectively, and dispersity Đ (by SEC) are listed in the table.

Series L1 copolymers	**$DP_{th,\ PEGMA\text{-}co\text{-}gMA}$ [-]**	**$\chi_{PEGMA\text{-}gMA}$ [%]**	**$M_{n,\ NMR}$ [Da]**	**$M_{n,\ NMR}$ [Da]**	**Đ [-]**
PCL_{30}-b-[$P(PEGMA)_6$-co-$PgMA_1$]	8	90	7030	12,266	1.3
PCL_{30}-b-$P(PEGMA)_9$	10	91	8030	14,300	1.3
PCL_{30}-b-$P(PEGMA)_{18}$	20	92	12,530	17,200	1.2
PCL_{30}-b-[$P(PEGMA)_{18}$-co-$PgMA_2$]	20	99	12,310	16,800	1.3
PCL_{30}-b-$P(PEGMA)_{27}$	30	90	17,020	22,200	1.2
PCL_{30}-b-[$P(PEGMA)_{26}$-co-$PgMA_3$]	30	96	16,950	21,800	1.2
PCL_{30}-b-[$P(PEGMA)_{35}$-co-$PgMA_3$]	40	96	21,450	25,000	1.1
PCL_{20}-b-[$P(PEGMA)_{12}$-co-$PgMA_3$]	18	85	8810	13,200	1.2
PCL_{20}-b-[$P(PEGMA)_{18}$-co-$PgMA_2$]	20	92	11,310	21,900	1.3
PCL_{40}-b-[$P(PEGMA)_{18}$-co-$PgMA_2$]	20	94	14,670	24,400	1.2
PCL_{50}-b-[$P(PEGMA)_{13}$-co-$PgMA_3$]	18	92	12,730	24,000	1.3
PCL_{50}-b-[$P(PEGMA)_{18}$-co-$PgMA_2$]	20	93	15,090	27,100	1.3
PCL_{30}-b-$PgMA_{20}$	20	99	6370	11,400	1.1
Series L2 copolymers	**$DP_{th,\ GMA\text{-}co\text{-}gMA}$ [-]**	**$\chi_{GMA\text{-}gMA}$ [%]**	**$M_{n,\ NMR}$ [Da]**	**$M_{n,\ SEC}$ [Da]**	**Đ [-]**
PCL_{30}-b-$PGMA_6$	8	80	4560	7400	1.2
PCL_{30}-b-[$PGMA_{10}$-co-$PgMA_2$]	15	85	5450	9900	1.3
PCL_{30}-b-[$PGMA_{15}$-co-$PgMA_3$]	20	92	6410	13,700	1.3
PCL_{30}-b-$PGMA_{23}$	25	92	7210	18,200	1.4
PCL_{30}-b-[$PGMA_{23}$-co-$PgMA_2$]	28	90	7530	19,400	1.2
PCL_{30}-b-[$PGMA_{27}$-co-$PgMA_3$]	35	87	8330	20,000	1.3
Series B1 copolymers	**$DP_{th,\ PEGMA\text{-}co\text{-}gMA}$ [-]**	**$\chi_{PEGMA\text{-}gMA}$ [%]**	**$M_{n,\ NMR}$ [Da]**	**$M_{n,\ SEC}$ [Da]**	**Đ [-]**
[PCL_{15}-b-[$P(PEGMA)_5$]]$_{30}$	5	99	57,890	77,300	1.3
[PCL_{15}-b-[$P(PEGMA)_7$-co-$PgMA_1$]]$_{30}$	10	86	58,680	76,300	1.2
[PCL_{15}-b-[$P(PEGMA)_{12}$-co-$PgMA_1$]]$_{30}$	15	91	62,040	80,500	1.2
[PCL_{15}-b-[$P(PEGMA)_{16}$]]$_{30}$	18	92	63,390	86,200	1.3
[PCL_{15}-b-[$P(PEGMA)_{17}$-co-$PgMA_2$]]$_{30}$	20	95	63,320	87,000	1.2
[PCL_{15}-b-[$P(PEGMA)_{20}$-co-$PgMA_3$]]$_{30}$	25	94	65,820	88,500	1.2

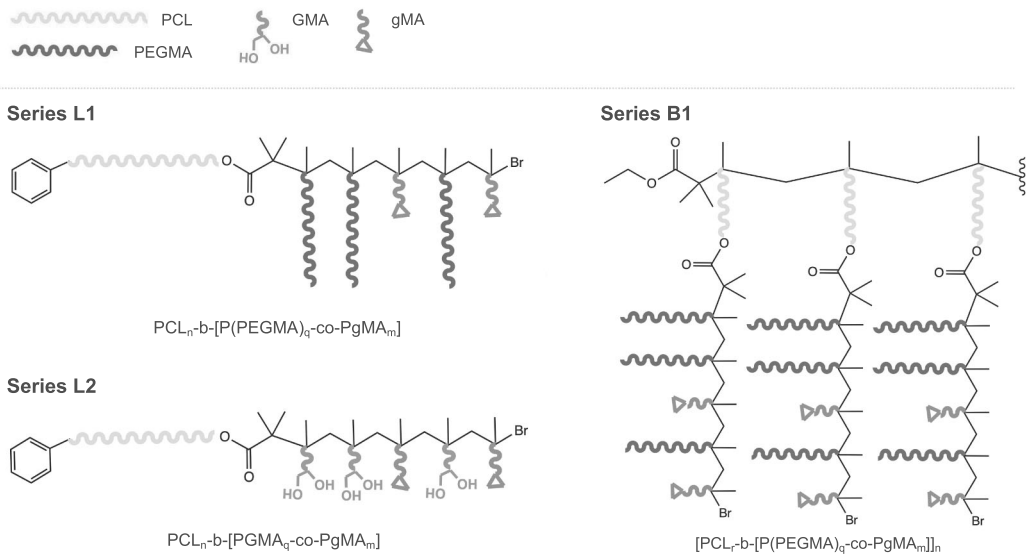

Fig. 3. Schematic representation of linear (Series L1 and L2) PCL_n-b-[$P(PEGMA)_q$-co-$PgMA_m$] or PCL_n-b-[$PGMA_q$-co-$PgMA_m$] copolymers and brush block (Series B1) $[PCL_r$-b-[$P(PEGMA)_q$-co-$PgMA_m]]_n$ copolymers.

this work, glycidyl units were successively exploited to be functionalized with thioacetic acid via a quantitative 'click' reaction. The number of gMA units was varied (ranging from 0 to 3) depending on the length of the hydrophilic block, in order to represent a maximum of 20 % of the hydrophilic monomeric units. To compare the properties of a functionalized macromolecule with its analogous (similar architecture and composition) which does not contain gMA, polymers constituted only by PCL, PEGMA or GMA were also synthesized (m = 0). On the other hand, a linear block copolymer with formula PCL_{30}-b-$PgMA_q$ was produced without PEGMA or GMA monomers (q = 0), to investigate how a heightened level of thiol functionalization (given m > 20 units) may alter the macromolecule properties, in particular its interactions with mucins and proteins.

A full list of the copolymers and their characterization data are summarized in Table 1, while a schematic representation of their topology is depicted in Fig. 3.

^{1}H NMR analysis was employed to follow each step of the polymer syntheses, and the NMR spectra of the different series of purified polymers are reported in the supporting information (*Figure S3)*, together with the SEC chromatograms for the different architectures and compositions (*Figure S4)*. The deviation of the M_n calculated by ^{1}H NMR from the value obtained by SEC was possibly due to the limits of the standard polystyrene calibration, and by the intrinsic limitation of SEC to determine the exact molar mass of comb-like and brush block copolymers, as observed in previous publications [1,13,35,60].

3.2. Post-polymerization functionalization with thiols

Copolymers presenting glycidyl methacrylate units were functionalized with TAA by ring opening of gMA epoxides [58]. The resulting post-polymerization modification [59,82] of glycidyl scaffolds featured the copolymers with newly formed $-SCOCH_3$ end-chain moieties. The strategy adopted represents an attractive functionalization route, as it is known to be fast, efficient and regioselective. Often been referred to as a 'click' reaction [83,84], it offers the opportunity to rationally design multifunctional polymers with tailored chemical structure and properties, according to the desired application of the final product [85]. While a variety of different functional groups can be grafted to the polymer via this method [86], in this case the conjugation with TAA was carried out to insert protected thiol groups.

The reaction was performed in THF in presence of TEA, to achieve 100 % conversion for a 1:1 molar ratio between the thiols and the epoxide functionalities. The scheme of the reaction is reported in Fig. 4, while in Fig. 5 the ^{1}H NMR (in DMSO-d_6) spectra recorded before and after the functionalization are also shown. The latter clearly highlighted that the peaks in the range of 2.5 – 3.0 ppm, corresponding to the protons of the epoxide group (labeled 'E' in Fig. 5.*a*), completely disappeared after the modification, with the simultaneous appearance of proton signals from the newly formed groups (labeled 'F' and 'G' in Fig. 5.*b*). More precisely, the peak at 2.3 ppm corresponds to the $-CH_3$ of the $-SCOCH_3$ moiety, while the one at 5.3 ppm indicates the hydroxyl

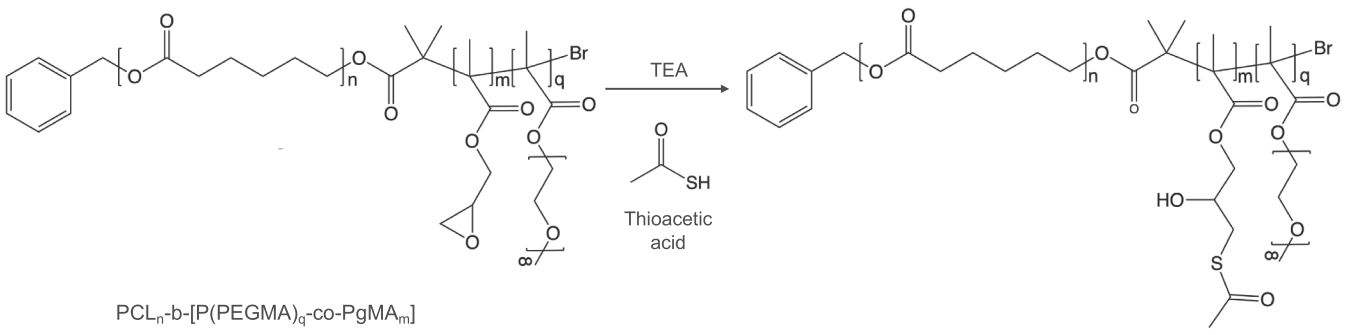

Fig. 4. Synthesis of PCL_n-b-[$P(PEGMA)_q$-co-$PgMA_m$] copolymers functionalized with thioacetic acid.

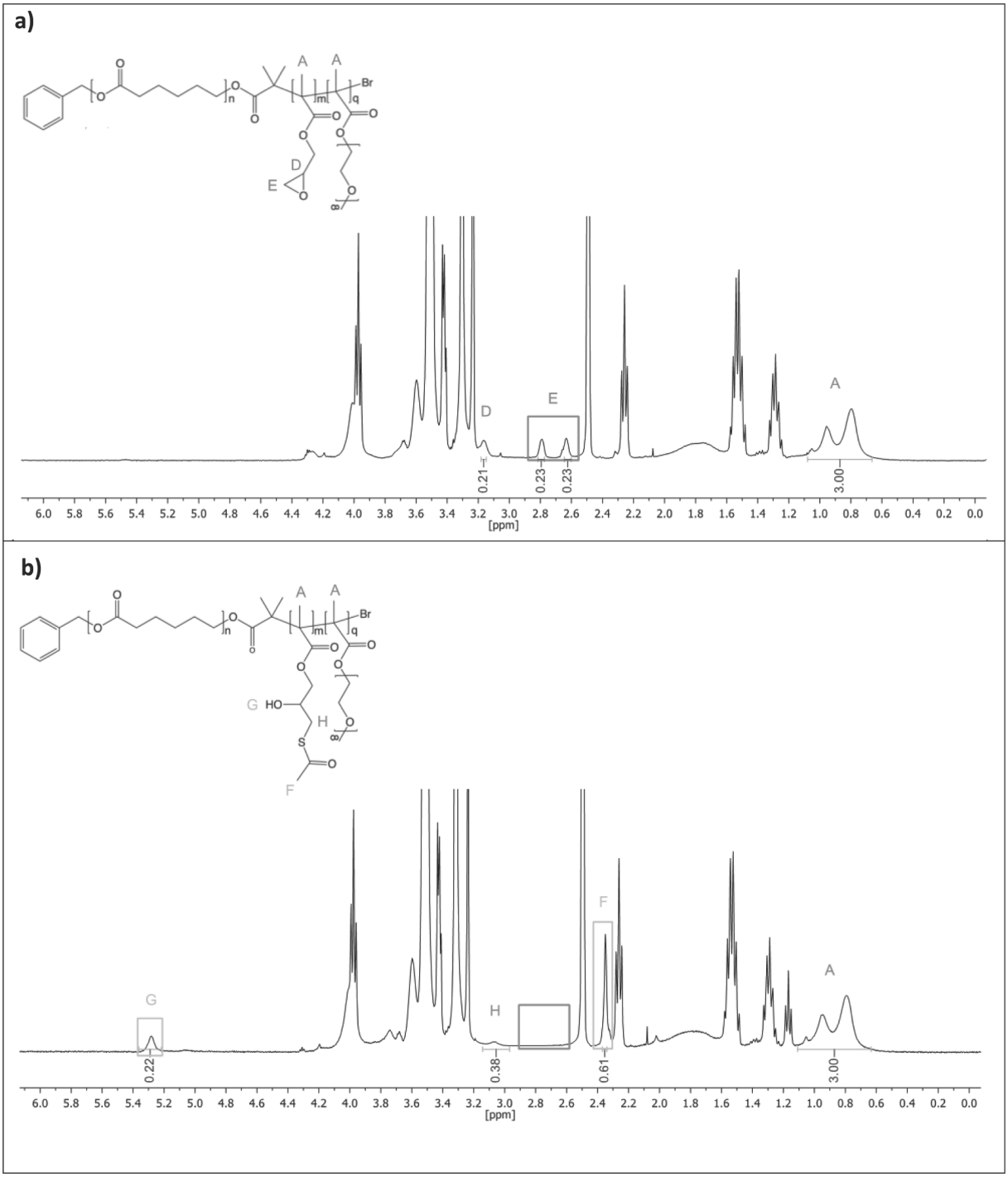

Fig. 5. ^{1}H NMR spectra (in DMSO-d_6) recorded **(a)** before and **(b)** after the epoxy ring opening reaction performed with thioacetic acid on PCL_{20}-b-[$P(PEGMA)_{12}$-co-$PgMA_3$] (gMA units represent the 20 % of P(PEGMA-co-gMA) copolymer).

group upon the ring-opening process. This confirmed a quantitative conversion of the epoxide groups into grafted thio-ester moieties.

3.3. Nanoparticles formulation and characterization

The NPs obtained from the synthesized macromolecules were prepared according to a nanoprecipitation/solvent (acetone) evaporation method [12,87,88]. The copolymers were designed to achieve a micellar structure with a core–shell morphology, where their inner core is constituted by the hydrophobic part of the amphiphiles, while the hydrophilic and functionalized components settle outside, in contact with the aqueous environment. The nanoassemblies were dispersed in PBS 10 mM at pH 7.4 and were characterized by DLS analysis at 25 °C. The full list of nanoparticles formulated, with their Z-average size and the corresponding polydispersity index, is reported in Table 2, while the size distribution curves are shown in *Figure S5* (*Supporting Information*). The average size was calculated with at least triplicates of each sample and reported with their corresponding standard deviation.

Regardless the polymer architecture and composition, the NPs presented a monomodal size distribution curve with a main peak covering 100 % of the scattering intensity, and a PdI $\leq$ 0.2, highlighting relatively narrow size distributions and homogeneous samples.

Table 2
Summary of properties of PCL_n-b-[P(PEGMA)$_q$-co-PgMA$_m$], PCL_n-b-[PGMA$_q$-co-PgMA$_m$] and [PCL_r-b-[P(PEGMA)$_q$-co-PgMA$_m$]]$_n$ suspensions (10 mg/mL in PBS 10 mM pH 7.4). Z-Average size and PdI evaluated by DLS analysis are reported in the table as mean values of measurements run at least in triplicates.

Series L1 NPs	Z-Av. Size [nm]	PdI [-]
PCL_{30}-b-[P(PEGMA)$_6$-co-PgMA$_1$]	85 ± 2	0.1
PCL_{30}-b-[P(PEGMA)$_9$]	79 ± 1	0.2
PCL_{30}-b-[P(PEGMA)$_{18}$]	51 ± 2	0.2
PCL_{30}-b-[P(PEGMA)$_{18}$-co-PgMA$_2$]	49 ± 1	0.2
PCL_{30}-b-[P(PEGMA)$_{27}$]	46 ± 1	0.2
PCL_{30}-b-[P(PEGMA)$_{26}$-co-PgMA$_3$]	45 ± 1	0.1
PCL_{30}-b-[P(PEGMA)$_{35}$-co-PgMA$_3$]	39 ± 1	0.1
PCL_{20}-b-[P(PEGMA)$_{18}$-co-PgMA$_2$]	31 ± 1	0.1
PCL_{40}-b-[P(PEGMA)$_{18}$-co-PgMA$_2$]	62 ± 2	0.2
PCL_{50}-b-[P(PEGMA)$_{13}$-co-PgMA$_3$]	82 ± 2	0.2
PCL_{50}-b-[P(PEGMA)$_{18}$-co-PgMA$_2$]	75 ± 2	0.2
Series L2 NPs	**Z-Av. Size [nm]**	**PdI [-]**
PCL_{30}-b-$PGMA_6$	96 ± 2	0.1
PCL_{30}-b-[$PGMA_{10}$-co-PgMA$_2$]	79 ± 2	0.2
PCL_{30}-b-[$PGMA_{15}$-co-PgMA$_3$]	53 ± 1	0.1
PCL_{30}-b-$PGMA_{23}$	49 ± 1	0.1
PCL_{30}-b-[$PGMA_{23}$-co-PgMA$_2$]	48 ± 1	0.2
PCL_{30}-b-[$PGMA_{27}$-co-PgMA$_3$]	44 ± 1	0.2
Series B1 NPs	**Z-Av. Size [nm]**	**PdI [-]**
[PCL_{15}-b-[P(PEGMA)$_5$]]$_{30}$	89 ± 2	0.1
[PCL_{15}-b-[P(PEGMA)$_7$-co-PgMA$_1$]]$_{30}$	42 ± 1	0.2
[PCL_{15}-b-[P(PEGMA)$_{12}$-co-PgMA$_1$]]$_{30}$	30 ± 1	0.2
[PCL_{15}-b-[P(PEGMA)$_{16}$]]$_{30}$	27 ± 1	0.2
[PCL_{15}-b-[P(PEGMA)$_{17}$-co-PgMA$_2$]]$_{30}$	26 ± 1	0.1
[PCL_{15}-b-[P(PEGMA)$_{20}$-co-PgMA$_3$]]$_{30}$	23 ± 1	0.2

Fig. 6 highlights how the size of the nanoassemblies varies as function of the polymer architecture, and by changing length and composition of the hydrophilic shell. For this comparison, the DP of the polyester main backbone was fixed to 30 units for both linear and brush block copolymers. As regards Series L1 and L2, PCL_{30}-b-[P(PEGMA)$_q$-co-PgMA$_m$] and PCL_{30}-b-[PGMA$_q$-co-PgMA$_m$] copolymers show the same size decreasing trend with the progressive increase in the DP of the hydrophilic block (m + p). No significant difference in size was recorded by substituting GMA to PEGMA macromonomer when the same design parameters (m and p) were maintained.

A similar tendency is presented by Series B1; a reduction in particles size was observed as consequence of extending the hydrophilic blocks, which favored the formation of smaller particles due to the increased hydrophilicity [1]. For brush block copolymers, this self-assembly pattern is more pronounced compared to linear copolymers, as a steeper reduction in particles size was observed with increasing PEGMA and gMA repeating units. Moreover, macromolecules with brushed hydrophobic block (Series B1) generally formed smaller colloids with respect to the ones assembled from copolymer with a linear lipophilic portion (Series L1 and L2). This behavior could be attributed to the stronger chain-chain interactions established during the micelles assembly given by the highly branched and packed structure of Series B1 copolymers [25]. Consequently, with this series it is possible to achieve particle size around 23 nm, whereas the smallest recorded for Series L is around 45 nm. Nonetheless, while conventional amphiphilic block copolymers form polymeric micelles above a certain critical micelle concentration (CMC), polymeric amphiphilic species with complex topologies may form unimolecular micelles which are stable upon high dilutions and can form below the CMC expected from the hydrophilic/lipophilic balance of the macromolecule [3,35].

By plotting the Z-Av. size recorded by DLS vs the DP of the hydrophilic block on a double logarithmic scale, a linear relationship between the two parameters was observed (*Figure S6, Supporting Information*). This indicates an exponential dependence of the Z-Av. size on the DP of the shell. In line with previous studies [89,90], scale factors linking the two variables were calculated and reported in *Equation (3)*.

$$Z-Av.\,Size\,[nm] = \begin{cases} 10^{2.3}(DP_{shell})^{-0.5} \textit{ for Series L copolymers} \\ 10^{2.5}(DP_{shell})^{-0.9} \textit{ for Series B copolymers} \end{cases} \quad (3)$$

As expected from the trend shown in Fig. 6, the equations describing the dependence of NPs size on DP_{shell} exhibit the same parameters for the L polymer series, regardless of the monomer constituting the shell. On the other hand, the scale factor calculated for the branched polymers is clearly different, reflecting a more rapid decrease in particle size as a function of DP_{shell}.

Fig. 7 presents the case of a growing hydrophobic block dimension with a fixed number of hydrophilic units. For PCL_n-b-[P(PEGMA)$_{18}$-co-PgMA$_2$] copolymers, higher is the DP of the hydrophobic block, larger are the nanoobjects formulated. This behavior is confirmed by the increase of the Z-average particle size from PCL_{20} to $PCL_{50,}$ and by the corresponding shift towards greater hydrodynamic diameters (D_h) of the

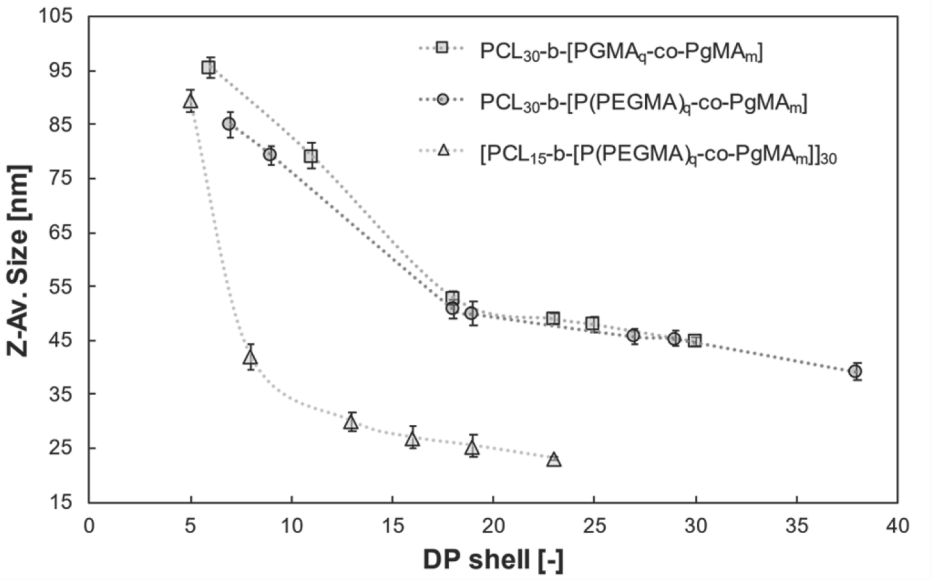

Fig. 6. NP size variation for Series L1 (blue), Series L2 (orange) and Series B1 (green) copolymers as a function of the number of monomeric units constituting their shell (m + q) with fixed hydrophobic block length (n = 30). Z-Average size evaluated by DLS analysis at 25 °C for suspensions (10 mg/mL) in PBS 10 mM pH 7.4. (For interpretation of the references to colour in this figure legend, the reader is referred to the web version of this article.)

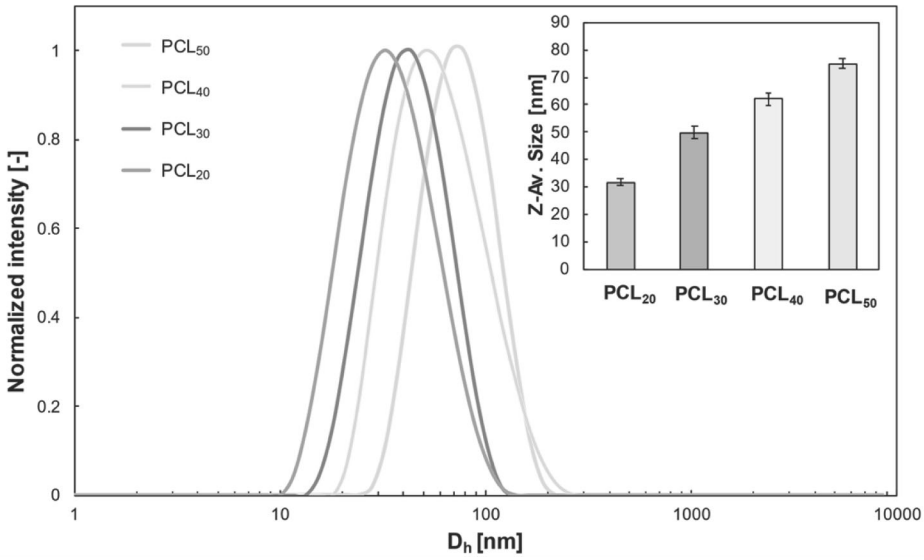

Fig. 7. NP size variation for Series L1 copolymers (PCL_n-b-[$P(PEGMA)_{18}$-co-$PgMA_2$]) as a function of the DP of the hydrophobic block constituting their core (n) with fixed hydrophilic fraction length (m + q = 20). Size distribution curve and Z-Average size (inset) evaluated by DLS analysis at 25 °C for suspensions (10 mg/mL) in PBS 10 mM pH 7.4.

size distribution curves (Fig. 7 inset). Thus, rising the DP of the main PCL_n backbone, the molecular rigidity of the polymer is strengthened, and an increase of lipophilic/hydrophilic ratio induce the formation of larger colloids.

Variation on the copolymer composition with the addition of glycidyl units within the hydrophilic blocks did not affect the particle size (Table 2 and Fig. 6).

Fig. 8 reports the TEM images obtained for both linear and branched copolymers.

The images revealed that no relevant differences in shape were observed when varying the macromolecular structure of the polymeric assembly. An almost spherical configuration was obtained for both PCL_n-b-[$P(PEGMA)_q$-co-$PgMA_m$] and [PCL_r-b-[$P(PEGMA)_q$-co-$PgMA_m$]]$_n$ copolymers. Nonetheless, the average diameter of the NPs was coherent with the ones previously determined via DLS analysis.

3.4. Drug encapsulation and DOX fluorescence analysis

Nanoparticles were loaded with a synthetic drug to evaluate whether the copolymers design parameters, and the resulting NP features, determine their encapsulation efficiency and drug loading performances. For this purpose, DOX was chosen as model drug, since it is one of the first line chemotherapeutic drugs [6,12] and require nanoencapsulation because of its prominent cardiac toxicity, short half-life, and low solubility in aqueous solution, which can hinder its therapeutic potential [6,12,60].

DOX was encapsulated by dissolving it in ultrapure water and adding it dropwise to the NP suspension. The adopted strategy differs from the typical methods used for DOX loading, as the use of organic solvents was avoided during the encapsulation procedure, in order to minimize any source of toxicity. In previous works [60] the amine group of DOX was firstly deprotonated in presence of TEA, thereby making the drug more hydrophobic and soluble in acetone (where the polymer was co-dissolved before nanoprecipitation in the aqueous phase). In this study, the encapsulation method exploited the effect of DOX dimerization in aqueous solution at physiological pH, so that the hydrophobic character of the resulting compound better allows the drug encapsulation within the polyester core of the NPs [77]. The mass ratio between DOX and the polymer (drug/polymer = 1/10 w/w) was maintained constant in the formulation, considering that 10 % w/w is far above the maximum percentage of drug that these kind of polymer systems are able to encapsulate [4,25]. The polymer mass was fixed at 10 mg/mL since previous studied demonstrated that the highest drug loadings were obtained at moderate polymer/drug concentrations (20 mg/mL and 10 mg/mL, mass drug/mass polymer = 1/10) [1]. The encapsulation efficiency (EE) and the nanoparticles drug loading (DL) were evaluated by fluorimetric analysis, thanks to the DOX intrinsic fluorescence. Table 3 summarizes the values of DL (%) and EE (%) obtained for the DOX-loaded nanoparticles formulated with the three different series of copolymers.

In terms of particle stability, the final DOX-loaded micelles presented a similar hydrodynamic diameter and size distribution curves (*Figure S7, Supporting Information*) to that of the unloaded polymers, suggesting that the drug encapsulation process, including the purification step, did not affect NP integrity (size variation within 1–2 nm were considered negligible for the purpose of this work). Fig. 9 shows the EE (%) and the corresponding DL (%) for the different copolymers synthetized. Concerning NPs with PEGMA repeating units as outer shell (Series L1, Fig. 9.*a*), the EE varied from 9.5 % to 15.3 %, with a slightly increasing trend by increasing the DP of the hydrophilic block. The same fashion is coherently followed also by the DL which reach its maximum value (1.52 ± 0.1) for the polymer PCL_{30}-b-[$P(PEGMA)_{35}$-co-$PgMA_3$]. A similar behavior is observed also when maintaining the same polymer architecture and design parameter but replacing PEGMA with GMA units (Series L2, Fig. 9.*b*). In this case, the increase in EE is more pronounced with longer hydrophilic blocks, ranging from 13.1 % to 31.3 %. The discrepancy in the EE and DL values obtained for the two aforementioned series may be attributed to the different steric hindrance of the hydrophilic monomeric units of the NP outer shell. PEGMA macromonomer are expected to form a significantly denser hydrophilic corona with respect to GMA monomer; therefore, the diffusion of the drug toward the hydrophobic core may be hindered when long hydrophilic side chains are present [91]. On the other hand, Fig. 9.*c* presents the DOX loading capacity of brush block copolymer (Series B1) having general formula [PCL_{15}-b-[$P(PEGMA)_q$-co-$PgMA_m$]]$_{30}$, where the DP of the main polyester backbone was fixed to 30 units, as for the linear copolymers. This series offered the highest drug loading with the best encapsulation performances, despite the reduced particles size, which is typically

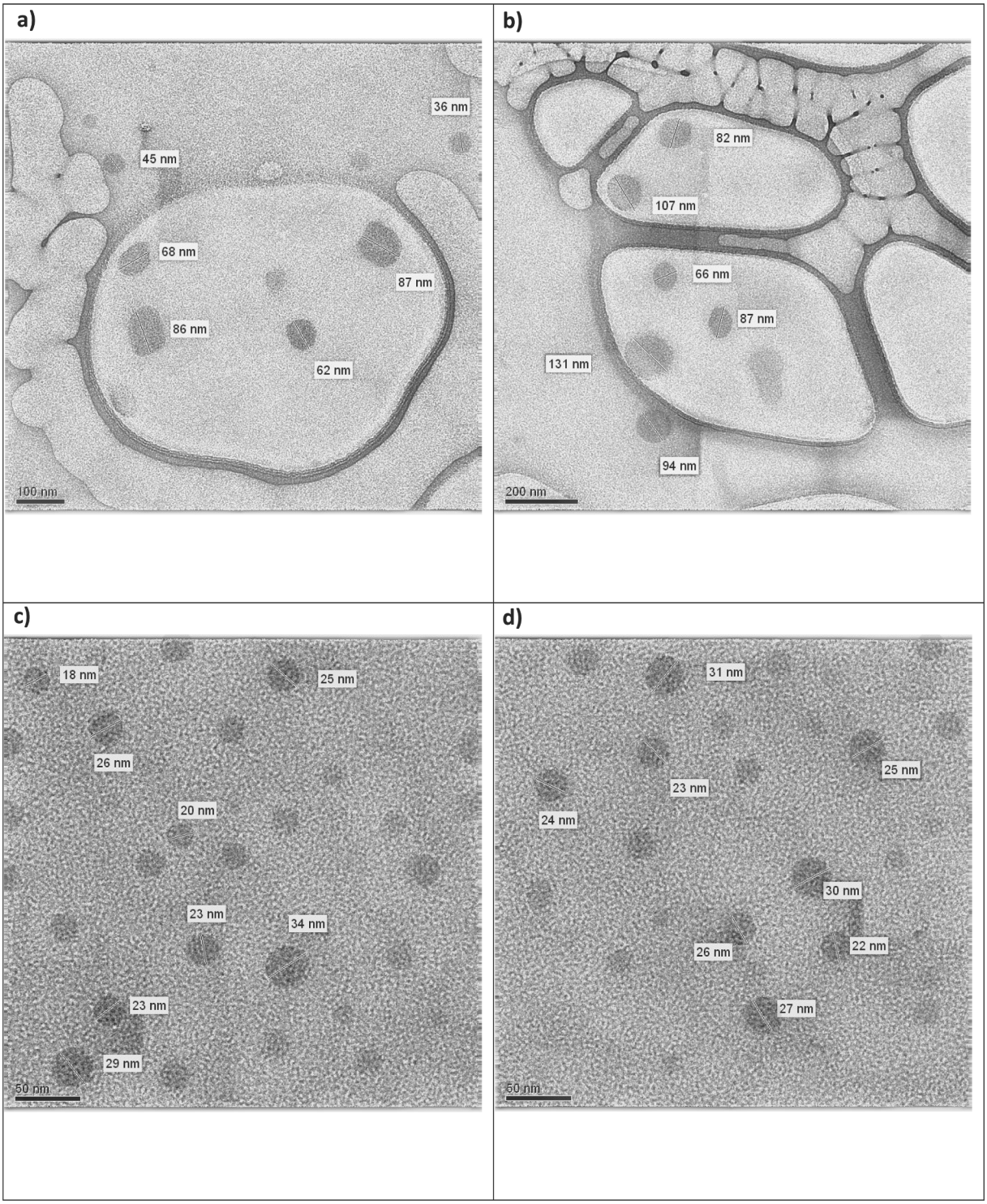

Fig. 8. TEM images representative of **(a-b)** linear block copolymers with formula PCL_n-b-[P(PEGMA)$_q$-co-PgMA$_m$] or PCL_n-b-[PGMA$_q$-co-PgMA$_m$] (Lacey carbon films on 400 mesh copper TEM grids, scale bar: 100 nm on the left and 200 nm on the right, respectively) and **(c-d)** brush block copolymers with formula [PCL_r-b-[P(PEGMA)$_q$-co-PgMA$_m$]]$_n$ (400 mesh copper TEM grids, scale bar: 50 nm). The images were processed for NPs size calculations with ImageJ software.

desirable for crossing biological barriers effectively [25]. The dense and highly packed NPs core obtained from these brush block copolymers may provide a stable environment for the encapsulated drug, minimizing DOX loss during the washing steps after the loading procedure. Fig. 9.*d* highlights the effect of increasing the PCL content (from PCL_{20} to PCL_{50}) in L1 copolymers while maintaining the same amount of hydrophilic units (m + q = 20). The outcomes revealed a remarkable loading improvement, given by the enhanced hydrophobicity of the nanosystem, which favored polymer-drug interaction and therefore drug loading. With a linear copolymer of 50 CL units, it is possible to obtain EE and DL value comparable to those obtained with brush block copolymers (Fig. 9.*c* and *9.d*).

Table 3
Summary of properties of PCL_n-b-[P(PEGMA)$_q$-co-PgMA$_m$], PCL_n-b-[PGMA$_q$-co-PgMA$_m$] and [PCL_r-b-[P(PEGMA)$_q$-co-PgMA$_m$]]$_n$ DOX-loaded nanoparticles (10 mg/mL in PBS 10 mM pH 7.4). Encapsulation efficiency (EE) and drug loading (DL) calculated by spectrofluorimetric analysis are reported in the table as mean values of measurements run at least in triplicates.

Series L1 NPs	**EE [%]**	**DL [%]**
PCL_{30}-b-[P(PEGMA)$_6$-co-PgMA$_1$]	9.5 ± 2.8	0.96 ± 0.3
PCL_{30}-b-[P(PEGMA)$_9$]	10.9 ± 1.6	1.12 ± 0.1
PCL_{30}-b-[P(PEGMA)$_{18}$]	12.6 ± 2.8	1.25 ± 0.5
PCL_{30}-b-[P(PEGMA)$_{18}$-co-PgMA$_2$]	14.1 ± 2.2	1.42 ± 0.2
PCL_{30}-b-[P(PEGMA)$_{27}$]	13.9 ± 1.7	1.38 ± 0.1
PCL_{30}-b-[P(PEGMA)$_{26}$-co-PgMA$_3$]	14.6 ± 2.4	1.46 ± 0.2
PCL_{30}-b-[P(PEGMA)$_{35}$-co-PgMA$_3$]	15.3 ± 1.3	1.52 ± 0.1
PCL_{20}-b-[P(PEGMA)$_{18}$-co-PgMA$_2$]	11.5 ± 1.3	1.16 ± 0.1
PCL_{40}-b-[P(PEGMA)$_{18}$-co-PgMA$_2$]	23.8 ± 1.3	2.41 ± 0.1
PCL_{50}-b-[P(PEGMA)$_{18}$-co-PgMA$_2$]	33.5 ± 1.3	3.35 ± 0.1
Series L2 NPs	**EE [%]**	**DL [%]**
PCL_{30}-b-$PGMA_6$	13.1 ± 1.6	1.32 ± 0.1
PCL_{30}-b-[$PGMA_{10}$-co-PgMA$_2$]	20.7 ± 0.7	2.08 ± 0.3
PCL_{30}-b-[$PGMA_{15}$-co-PgMA$_3$]	24.5 ± 1.7	2.46 ± 0.2
PCL_{30}-b-$PGMA_{23}$	27.5 ± 1.3	2.78 ± 0.1
PCL_{30}-b-[$PGMA_{23}$-co-PgMA$_2$]	26.9 ± 2.3	2.71 ± 0.2
PCL_{30}-b-[$PGMA_{27}$-co-PgMA$_3$]	31.3 ± 0.9	3.12 ± 0.1
Series B1 NP	**EE [%]**	**DL [%]**
[PCL_{15}-b-[P(PEGMA)$_5$]$_{30}$	16.8 ± 1.8	1.70 ± 0.3
[PCL_{15}-b-[P(PEGMA)$_7$-co-PgMA$_1$]]$_{30}$	18.7 ± 2.3	1.86 ± 0.2
[PCL_{15}-b-[P(PEGMA)$_{12}$-co-PgMA$_1$]]$_{30}$	20.1 ± 1.3	2.00 ± 0.1
[PCL_{15}-b-[P(PEGMA)$_{16}$]$_{30}$	28.7 ± 2.1	2.86 ± 0.2
[PCL_{15}-b-[P(PEGMA)$_{17}$-co-PgMA$_2$]]$_{30}$	32.2 ± 2.3	3.22 ± 0.2
[PCL_{15}-b-[P(PEGMA)$_{20}$-co-PgMA$_3$]]$_{30}$	33.3 ± 1.4	3.32 ± 0.1

3.5. Thiols deprotection on functionalized nanoparticles and size reduction effect

After the nanoprecipitation of thio-functionalized copolymers, the $-SCOCH_3$ moieties, which were introduced through the functionalization of the glycidyl units, were deprotected to yield free −SH groups within the NPs shell (*Figure S8, Supporting Information*).

The hydrolysis reaction was performed in slightly basic condition (pH = 9) [61] to prevent polymer degradation and minimize adverse effects on NP stability. The progression of the deprotection reaction was monitored by means of Ellman's reagent (DTNB) assay [79], withdrawing aliquots of the reaction mixture at different time points. The same analysis was also performed by pre-treating each aliquot with an immobilized TCEP disulfide reducing gel, to reduce possible disulfides formed before the test, which may alter the quantification of deprotected thiols. Fig. 10 shows the ratio (as percentage) of free thiols detected at each time point with respect the total mol of sulfhydryls available with a complete deprotection of $-SCOCH_3$ groups (according to the number of glycidyl repeating units present in the mass of treated polymer). When the sample was treated with TCEP reducing gel, after 30 min of hydrolysis 100 % thiols were deprotected, and the plateau of the % thiol deprotection curve was maintained for the subsequent time points. The profile of the samples not reduced with TCEP overlapped the aforementioned curve until 20 min of reaction, which corresponds to a percentage of free −SH equal to 80 %. Afterwards, the percentage of free thiols detected was gradually reduced, reaching approximately 40 % at 75 min. This behavior confirmed the progressive formation of disulfide bridges between free −SH groups over time. The depicted profile offers insight into the rate at with this process occurs under the selected experimental conditions of pH and temperature.

The benefit of having protected thiols lies in preventing oxidation or undesirable interactions until deprotection is required for specific applications. The system is therefore more stable compared to an analogous one obtained from copolymers functionalization with molecules containing free thiols [71]. The formation of disulfide bridges within the hydrophilic corona is beneficial in view of employing these NPs as drug delivery nanocarriers. Indeed, additional covalent intramolecular interactions may confer strength and enhanced stability to the NPs, also providing an additional tool to tune their size and self-assembly behavior. The effect of S-S bond formation on NPs was assessed via DLS analysis, by measuring their size before the deprotection reaction (as described in the previous section) and at different time points after the hydrolysis of the thioesters. Fig. 11 shows the outcome of this comparison for PCL_{50}-b-[P(PEGMA)$_{13}$-co-PgMA$_3$] copolymer: by resuspending the thiolated nanoparticles in PBS 10 mM at pH 7.4, they became progressively smaller over time, due to disulfide formation. At 24 h after thiol deprotection, around 25 % of size reduction was measured for the NPs analyzed, and no relevant variation were noticed for the successive time points. Thus, when all the free thiols are oxidized to disulfides, the nanosystems reach an equilibrium, with the consequent shrinking of the NPs corona. The same size reduction profile over time was observed during several tests, confirming good reproducibility and control over NPs dimension at a fixed polymer degree of functionalization (as demonstrated by the error bars always < 2 %), together with good statistical significance ($P < 0.01$). Conducted tests also demonstrated that once free −SH groups are present, they preferentially tend to form intramolecular bonds with other sulfur groups within the same structure, rather than forming long-range interactions with sulfur groups belonging to other NPs. This behavior was confirmed by the fact that the final colloidal suspension exhibited smaller dimensions compared to the initial one, while maintaining the profile of the DLS curves unchanged. This outcome would not have been possible if aggregates resulting from the fusion of multiple NPs had formed.

Functionalizing NPs with thiols not only enables us to utilize the corona shirking effect, reducing their tendency to collapse and degrade in biological fluids, but also provides a tool for fine-tuning their dimensions beyond the initial synthesis design. This effect can control and reduce the particle size from linear polymers with extensive hydrophobic cores, which enhance encapsulation but result in larger particle sizes, as previously discussed. Thus, forming disulfide bridges can contract NP dimensions after formulation and drug loading, achieving the desired physicochemical properties for specific applications. Additionally, this approach allows us to achieve similar features and performance between linear and brushed copolymers. The latter are optimal ultrasmall delivery vehicles, although they require more complex synthesis procedures.

3.6. Thiolated nanoparticles adhesion on mucins and proteins

Thiolated polymers generally show mucoadhesive properties, resulting from their ability to form strong covalent bonds with cysteine-rich subdomains of mucus glycoproteins, by means of a disulfide-thiol exchange process [92]. Such interactions could ensure marked adhesion with mucosal tissues, leading to the development of drug delivery platforms with increased retention time and localized release via specific administration routes (as through the gastrointestinal tract, eye, nose, and lung) [34,72]. However, in some cases mucous adhesion is not auspicial since nanocarriers adsorption on non-targeted tissue may impede their drug release at the predetermined site. Therefore, depending on the specific application, it is fundamental to identify the optimal polymer topology and the degree of functionalization with free sulfhydryl groups to ensure the desired behavior of the nanoassemblies when administered for drug delivery purposes.

Mucus interaction of three different polymers was tested: PCL_{30}-b-P(PEGMA)$_{18}$ with no functional glycidyl units (POL1), thus not presenting any free −SH groups; PCL_{30}-b-[P(PEGMA)$_{18}$-co-PgMA$_2$] where glycidyl monomers were functionalized with thioacetic acid (POL2) to provide deprotected −SH functionalities corresponding to 10 % of the hydrophilic shell of the nanoparticles; and PCL_{30}-b-$PgMA_{20}$ without PEGMA units, where glycidyl functionalized with thiols entirely constitute the hydrophilic block of the copolymer (POL3). Glycidyl functionalization and consequent thiols deprotection were performed employing the same

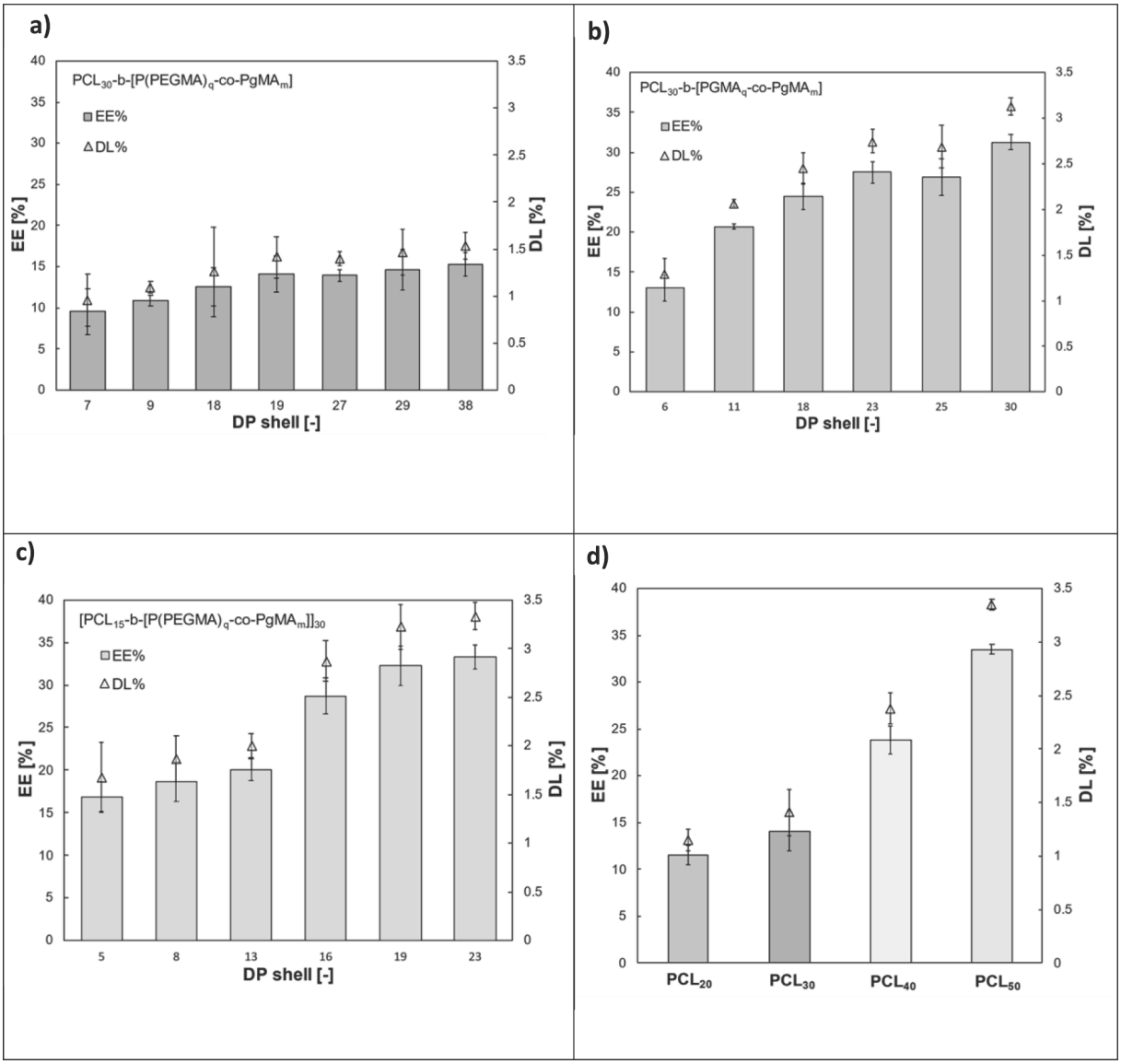

Fig. 9. EE (bars) and DL (triangles) variation for NPs obtained from **(a)** Series L1, **(b)** Series L2 and **(c)** Series B1 copolymers, as a function of the number of monomeric units constituting their shell (m + q), with fixed hydrophobic block length (n = 30). **(d)** EE (bars) and DL (triangles) variation for Series L1 copolymers as a function of the DP of the hydrophobic block constituting their core (n) with fixed hydrophilic fraction length (m + q = 20). Data were evaluated by fluorimetric analysis at 255 nm for DOX-loaded nanoparticles (10 mg/mL) in PBS 10 mM pH 7.4.

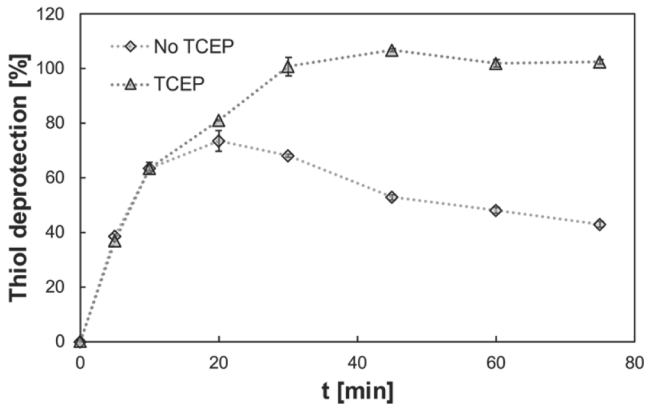

Fig. 10. Thiol deprotection kinetic profile recorded via Ellman's reagent assay, performing (tringles) or not (rhombus) a reducing treatment (TCEP gel) against the formation of S-S covalent bonds.

procedures described by the previous sections. After thiols deprotection, the same amount of the three copolymers was mixed with a fixed mass of mucin from porcine stomach in PBS buffer at pH 7.4. The samples obtained were analyzed at DLS to measure their scattering intensity, the average size of the assembly formed (Z-Av. Size) and the size distribution curve. The optical density (O.D.) of these samples was also evaluated via spectrophotometric analysis at 420 nm. All the measurements were compared with negative control tests on samples containing either mucins or each of the three polymers alone, at the same concentration used for the previously mentioned specimens. No relevant differences were experienced in terms of derived count rate, Z-Av. Size and O.D. when repeating the analysis 1 h or 2 h after the polymer-mucins mixing. Fig. 12 shows the scattering intensity and O.D. variation within the different suspensions, while Table 4 summarizes the average size and the percentage of the scattering intensity (I%) of the main peak detected in the samples analyzed. Fig. 12 highlights that mixing mucins with a polymer lacking free thiols (POL1) results in no difference in the scattering intensity between the NPs alone and the polymer-mucin mixture (POL1 + MUC). This indicates no aggregates were formed and no

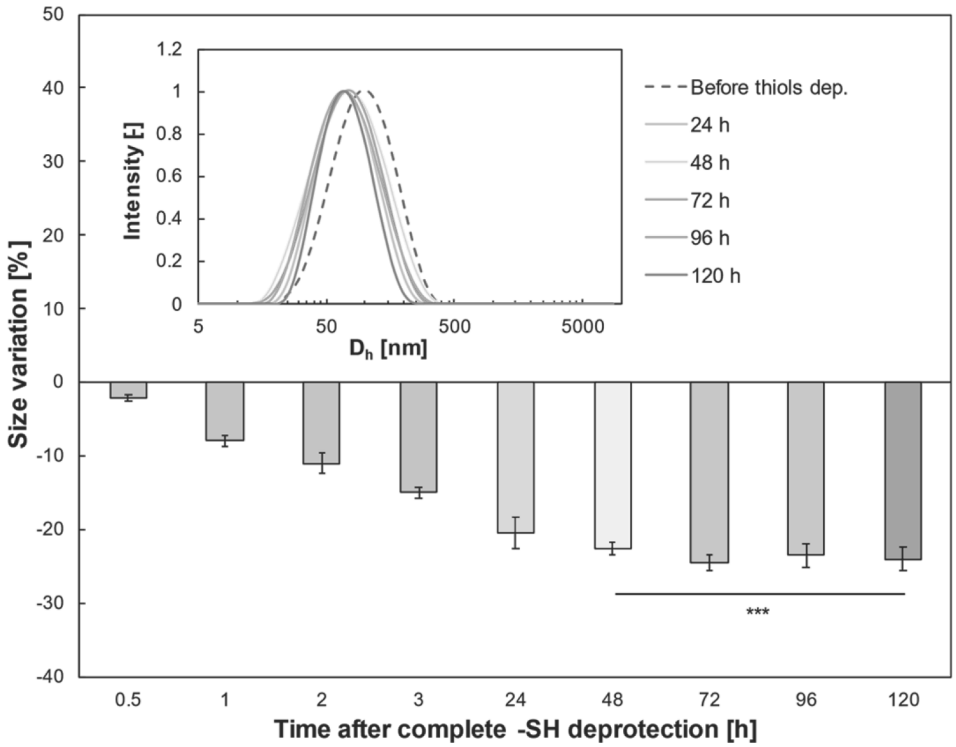

Fig. 11. Percentage of PCL_{50}-b-[$P(PEGMA)_{13}$-co-$PgMA_3$] NP size reduction (after performing thiols deprotection reaction) due to the formation of S-S bridges within micelles corona (N = 3, P < 0.01). Size distribution curve (inset) and Z-Average size used to calculate % size reduction were evaluated by DLS analysis at 25 °C for suspensions in PBS 10 mM pH 7.4.

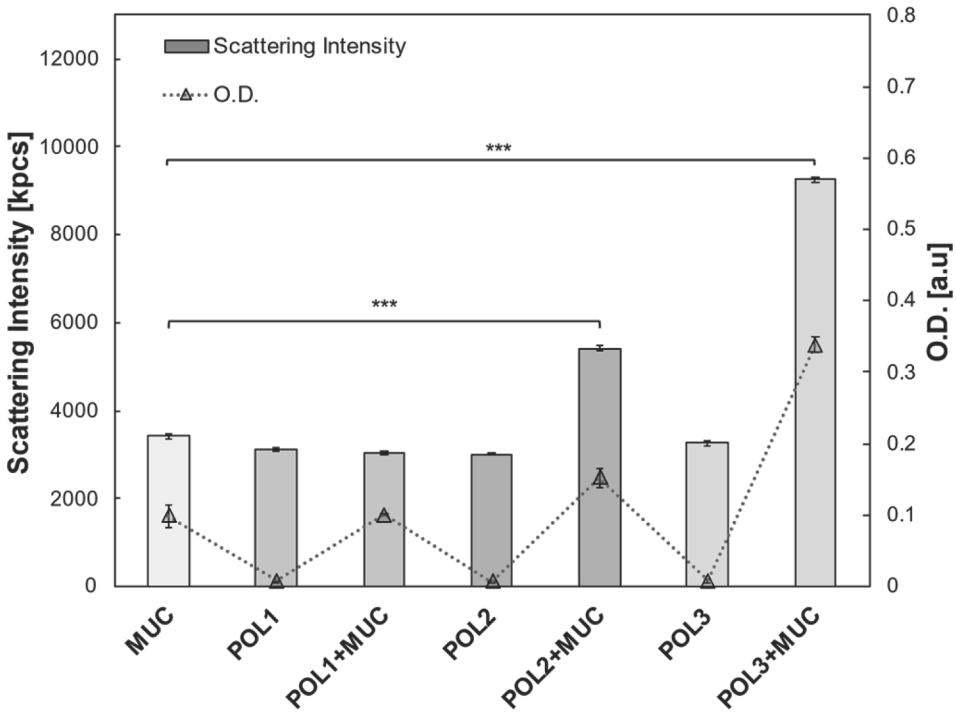

Fig. 12. Average scattering intensity measured by DLS analysis and optical density (O.D.) acquired via UV–Vis spectrophotometry (420 nm) of PCL_{30}-b-[$P(PEGMA)_{18}$] (POL1), thiolated PCL_{30}-b-[$P(PEGMA)_{18}$-co-$PgMA_2$] (POL2), thiolated PCL_{30}-b-$PgMA_{20}$ (POL3), mucin and their mixtures in PBS 10 mM pH 7.4. (N=3, P<0.001).

interactions occurred between the polymer and mucins. On the other hand, when the same test was conducted on particles functionalized with thiols (POL2), a change was observed between their scattering intensity and the one of the suspensions they form with mucins (POL2 + MUC). The difference is statistically significant even when the comparison was performed with mucins alone (scattering intensity slightly higher than that of the polymeric suspension). The observed difference confirmed that polymers with free thiols were able to interact with

Table 4
Summary of Z-Average ize and PdI of mucins, polymers, and their relative mixtures in PBS 10 mM pH 7.4. D_h represents the mean hydrodynamic diameter of the main peak observed in the intensity size distribution curve, while I% indicates its related mean intensity percentage. All the data were evaluated by DLS analysis and are reported in the table as the mean values of measurements run in triplicate.

Abbreviations	Samples	Z-Av. Size [nm]	PdI [-]	D_h [nm]	I [%]
MUC	Mucin	907 ± 52	0.98	812 ± 30	73
POL1	PCL_{30}-b-[P$(PEGMA)_{18}$]	52 ± 1	0.21	58 ± 2	99
POL1 + MUC	PCL_{30}-b-[P$(PEGMA)_{18}$] + Mucin	55 ± 1	0.32	70 ± 5	90
POL2	PCL_{30}-b-[P$(PEGMA)_{18}$-co-$PgMA_2$]	50 ± 0.5	0.17	55 ± 2	100
POL2 + MUC	PCL_{30}-b-[P$(PEGMA)_{18}$-co-$PgMA_2$] + Mucin	228 ± 55	0.70	466 ± 20	60
POL3	PCL_{30}-b-$PgMA_{20}$	77 ± 11	0.73	164 ± 10	84
POL3 + MUC	PCL_{30}-b-$PgMA_{20}$ + Mucin	1388 ± 21	0.78	667 ± 20	96

mucins, thus forming larger colloids. Indeed, as their size is increased, they coherently exhibited higher scattering intensity. A similar phenomenon was observed using the block copolymer consisting solely of PCL and PgMA fully functionalized with thioacetic acid (POL3). A significantly high degree of thiol functionalization of the overall macromolecule (10-fold higher with respect to POL2) induced strong interactions with the mucins present in the sample, leading to the formation of agglomerates of considerably larger sizes. This was confirmed by a significantly higher scattering intensity than those recorded from the other samples. Thus, despite the steric hindrance of PEGMA macromonomers constituting the NP shell, these findings demonstrated that thiol-functionalized nanocarriers show favorable interactions with mucins, in contrast to their non-functionalized counterparts. Although the analysis of the derived scattering intensity was used only as a preliminary and simple metric for examining the binding phenomena between thiolated polymers and mucins, without employing more precise methods for characterizing binding affinity — such as isothermal titration calorimetry (ITC), viscometry, or asymmetrical flow field-flow fractionation (AsFFF) [93]— this approach revealed that a rational polymer structure design and a precise degree of functionalization can lead to the development of nanocarriers that selectively bind to mucin layers, tailored to the desired drug delivery application.

Similarly, the interaction between thiolated macromolecules and bovine serum albumin (BSA) was also investigated. BSA, as a model protein, is representative of the most abundant proteins in biological fluids, specifically in blood plasma. The intention was to understand if, based on the number of free thiols present in their molecular structure, these polymeric nanomaterials were more inclined to form intramolecular disulfide bridges or had the tendency to interact with disulfide-rich subdomains of the protein. Fig. 13 shows the average

Table 5
Summary of Z-Average size and PdI of BSA, polymers, and their relative mixtures in PBS 10 mM pH 7.4. D_h represents the mean hydrodynamic diameter of the main peak observed in the intensity size distribution curve, while I% indicates its related mean intensity percentage. All the data were evaluated by DLS analysis and are reported in the table as the mean values of measurements run in triplicate.

Abbreviations	Samples	Z-Av. Size [nm]	PdI [-]	D_h [nm]	I [%]
BSA	BSA	10 ± 0.2	0.28	9 ± 1	87
POL1	PCL_{30}-b-[P$(PEGMA)_{18}$]	52 ± 1	0.21	58 ± 2	99
POL1 + BSA	PCL_{30}-b-[P$(PEGMA)_{18}$] + BSA	31 ± 0.1	0.51	60 ± 5	80
POL2	PCL_{30}-b-[P$(PEGMA)_{18}$-co-$PgMA_2$]	50 ± 0.5	0.17	55 ± 2	100
POL2 + BSA	PCL_{30}-b-[P$(PEGMA)_{18}$-co-$PgMA_2$] + BSA	15 ± 0.3	0.41	10 ± 1	60
POL3	PCL_{30}-b-$PgMA_{20}$	77 ± 11	0.73	164 ± 10	84
POL3 + BSA	PCL_{30}-b-$PgMA_{20}$ + BSA	15 ± 5	0.22	9 ± 2	90

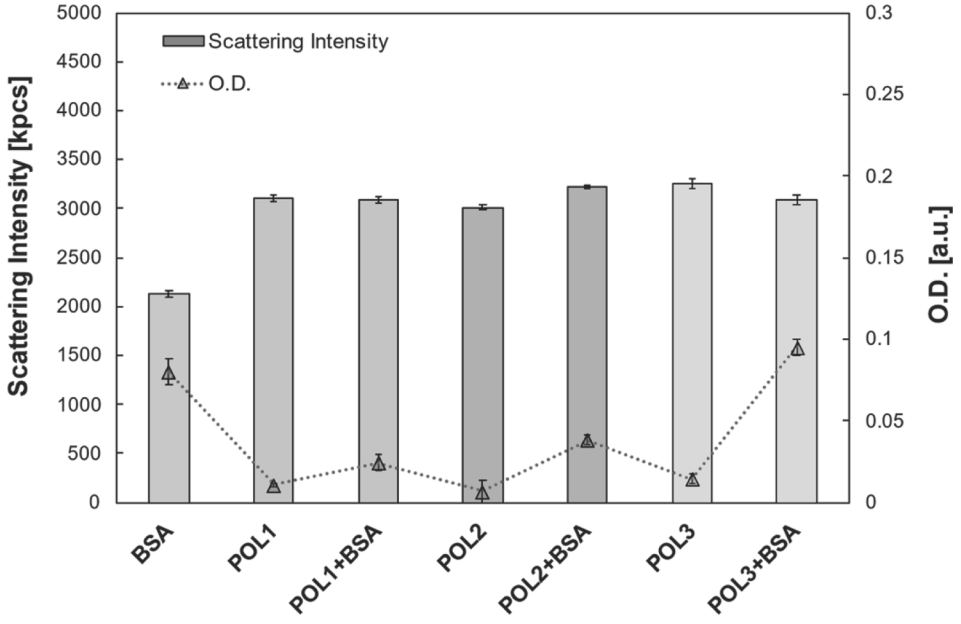

Fig. 13. Average scattering intensity measured by DLS analysis and optical density (O.D.) acquired via UV–Vis spectrophotometry (420 nm) of PCL_{30}-b-[P$(PEGMA)_{18}$] (POL1), thiolated PCL_{30}-b-[P$(PEGMA)_{18}$-co-$PgMA_2$] (POL2), thiolated PCL_{30}-b-$PgMA_{20}$ (POL3), BSA and their mixtures in PBS 10 mM pH 7.4.

scattering intensity and O.D. variations within the different polymer-BSA suspensions, while Table 5 summarizes the average size and the percent scattering intensity (I%) of the main peak detected in the samples analyzed. In this context, analyzing both thiolated nanoparticles and those without functionalization, the difference between the scattering intensity of the polymer suspensions and that of their mixtures with BSA was found to be negligible. Regarding the PCL_{30}-$PgMA_{20}$ block copolymer, although the photon count rate resulting from the mixing with BSA is higher than that of the polymer alone, it is still not significant compared to the photon count rate of the BSA solution in PBS. Therefore, the presence of thiols along the polymer structure does not appear to alter the interaction with BSA, and thus should not promote the absorption of proteins present in biological fluids.

4. Conclusions

A library of amphiphilic copolymers incorporating PCL and either P(PEGMA) or PGMA was synthesized via ROP and ATRP. The aim was to investigate how variations in macromolecular design and the independent adjustment of architectural parameters affect self-assembly, nanoparticles size, drug loading capabilities, and bioactivity. Firstly, linear and brush block copolymers presenting variable hydrophobic and hydrophilic block lengths were examined to investigate their NPs formation in aqueous dispersion.

Size distribution analysis confirmed that NPs size varies with polymer architecture, specifically with the hydrophilic shell length and composition. Both linear and brush block copolymers show reduced size with longer hydrophilic blocks. Brush block copolymers consistently form smaller nanoparticles due to stronger chain interactions, offering potential advantages in crossing biological barriers. While the hydrophobic block length of the copolymers has detectable effect on the diameter of the nanocarrier, the addition of functional glycidyl units within the hydrophilic block does not significantly affect particles size.

Nanoparticles were loaded with DOX to evaluate encapsulation efficiency and drug loading. Results showed that copolymer design parameters significantly affect drug loading performance. Brush block copolymers exhibited the highest efficiency, offering potential for optimized drug delivery systems with increased stability and reduced size. These results highlight the importance of polymer architecture in nanocarrier design, and how a proper selection of the macromolecular topology may allow a fine tuning of the physicochemical properties of these nanomaterials.

After copolymers functionalization with thioacetic acid, free −SH groups were successfully obtained by deprotecting the $-SCOCH_3$ moiety under slightly basic conditions to prevent polymer degradation. Intramolecular disulfide networks provide an additional tool to enhance stability and reduce the final size of the nanocarriers, regardless of the design parameters set during the synthesis. This approach could be exploited to design NPs with a larger hydrophobic core (desirable to maximise drug encapsulation), while maintaining the characteristics of ultra-small delivery vehicles, such as those obtained with brushed copolymers (which are more complex to synthesize).

These polymers also exhibited mucoadhesive properties by forming covalent bonds with cysteine-rich mucus glycoproteins. The use of biodegradable thiolated nanomaterials has the potential to significantly impact drug delivery through mucosal tissues. This is due to their ability to improve targeted drug delivery and prolong drug retention, ultimately resulting in improved therapeutic outcomes. However, unintended mucosal adhesion may also impede targeted drug delivery in some cases. Therefore, the degree of thiol functionalization may be tuned to predict the behavior of the NPs and thus control whether they will interact with mucosal tissues, depending on the specific application and the desired effect. This study assessed the interaction of three polymers with mucins and BSA, revealing that thiol-functionalized polymers increased mucin binding but did not significantly alter BSA interaction, suggesting selective application potential in drug delivery.

CRediT authorship contribution statement

Ilaria Porello: Writing – review & editing, Writing – original draft, Methodology, Investigation, Data curation, Conceptualization. **Federico Stucchi:** Investigation. **Giulia Sbaruffati:** Investigation. **Francesco Cellesi:** Writing – review & editing, Writing – original draft, Supervision, Methodology, Investigation, Funding acquisition, Data curation, Conceptualization.

Declaration of competing interest

The authors declare that they have no known competing financial interests or personal relationships that could have appeared to influence the work reported in this paper.

Data availability

Data will be made available on request.

Appendix A. Supplementary material

Supplementary data to this article can be found online at https://doi.org/10.1016/j.eurpolymj.2024.113455.

References

[1] W. Celentano, S. Ordanini, R. Bruni, L. Marocco, P. Medaglia, A. Rossi, S. Buzzaccaro, F. Cellesi, Complex poly(ε-caprolactone)/poly(ethylene glycol) copolymer architectures and their effects on nanoparticle self-assembly and drug nanoencapsulation, Eur. Polym. J. 144 (2021), https://doi.org/10.1016/j.eurpolymj.2020.110226.
[2] W. Celentano, J. Battistella, I.P. Silvestri, R. Bruni, X. Huang, M. Li, P. Messa, S. Ordanini, F. Cellesi, Engineered polyester-PEG nanoparticles prepared through a "grafting through" strategy and post-functionalization via Michael type addition, React. Funct. Polym. 131 (2018) 164–173, https://doi.org/10.1016/j.reactfunctpolym.2018.07.011.
[3] S. Ordanini, F. Cellesi, Complex polymeric architectures self-assembling in unimolecular micelles: Preparation, characterization and drug nanoencapsulation, Pharmaceutics 10 (2018), https://doi.org/10.3390/pharmaceutics10040209.
[4] C. Colombo, M. Li, S. Watanabe, P. Messa, A. Edefonti, G. Montini, D. Moscatelli, M.P. Rastaldi, F. Cellesi, Polymer nanoparticle engineering for podocyte repair: From in vitro models to new nanotherapeutics in kidney diseases, ACS Omega 2 (2017) 599–610, https://doi.org/10.1021/acsomega.6b00423.
[5] Z. Su, R. Zhang, X.Y. Yan, Q.Y. Guo, J. Huang, W. Shan, Y. Liu, T. Liu, M. Huang, S. Z.D. Cheng, The role of architectural engineering in macromolecular self-assemblies via non-covalent interactions: A molecular LEGO approach, Prog. Polym. Sci. 103 (2020), https://doi.org/10.1016/j.progpolymsci.2020.101230.
[6] M. Han, Diao, Fu, Hu, Jiang, Tsutsumi, Wei, Chen, J.-Q. Gao, Doxorubicin-loaded PEG-PCL copolymer micelles enhance cytotoxicity and intracellular accumulation of doxorubicin in adriamycin-resistant tumor cells, Int J Nanomedicine (2011) 1955. DOI: 10.2147/ijn.s23099.
[7] R. Joy, J. George, F. John, Brief outlook on polymeric nanoparticles, micelles, niosomes, hydrogels and liposomes: Preparative methods and action, ChemistrySelect 7 (2022), https://doi.org/10.1002/slct.202104045.
[8] C. Conte, I. D'angelo, A. Miro, F. Ungaro, F. Quaglia, Send Orders for Reprints to reprints@benthamscience.net PEGylated Polyester-Based Nanoncologicals, 2014.
[9] Y. Yi, G. Lin, S. Chen, J. Liu, H. Zhang, P. Mi, Polyester micelles for drug delivery and cancer theranostics: Current achievements, progresses and future perspectives, Mater. Sci. Eng. C 83 (2018) 218–232, https://doi.org/10.1016/j.msec.2017.10.004.
[10] Z. Liu, X. Ji, D. He, R. Zhang, Q. Liu, T. Xin, Nanoscale drug delivery systems in glioblastoma, Nanoscale Res. Lett. 17 (2022), https://doi.org/10.1186/s11671-022-03668-6.
[11] A.G. Niculescu, A.M. Grumezescu, Novel tumor-targeting nanoparticles for cancer treatment— A review, Int. J. Mol. Sci. 23 (2022), https://doi.org/10.3390/ijms23095253.
[12] X. Zhang, J. Cheng, R. Zhuo, Amphiphilic hyperbranched polymers with a biodegradable hyperbranched poly(ϵ-caprolactone) core prepared from homologous AB2 macromonomer, RSC Adv. 6 (2016) 52334–52338, https://doi.org/10.1039/c6ra08531h.
[13] W. Celentano, G. Neri, F. Distante, M. Li, P. Messa, C. Chirizzi, L. Chaabane, F. De Campo, P. Metrangolo, F. Baldelli Bombelli, F. Cellesi, Design of fluorinated hyperbranched polyether copolymers for 19F MRI nanotheranostics, Polym Chem 11 (2020) 3951–3963. DOI: 10.1039/d0py00393j.
[14] G. Neri, G. Mion, A. Pizzi, W. Celentano, L. Chaabane, M.R. Chierotti, R. Gobetto, M. Li, P. Messa, F. De Campo, F. Cellesi, P. Metrangolo, F. Baldelli Bombelli, Fluorinated PLGA Nanoparticles for Enhanced Drug Encapsulation and 19F NMR

Detection, Chemistry - A European Journal 26 (2020) 10057–10063. DOI: 10.1002/chem.202002078.
[15] P. Lagarrigue, F. Moncalvo, F. Cellesi, Non-spherical polymeric nanocarriers for therapeutics: The effect of shape on biological systems and drug delivery properties, Pharmaceutics 15 (2023), https://doi.org/10.3390/pharmaceutics15010032.
[16] J. Grundler, K. Shin, H.W. Suh, M. Zhong, W.M. Saltzman, Surface topography of polyethylene glycol shell nanoparticles formed from bottlebrush block copolymers controls interactions with proteins and cells, ACS Nano 15 (2021) 16118–16129, https://doi.org/10.1021/acsnano.1c04835.
[17] W. Zhang, Y. Li, L. Liu, Q. Sun, X. Shuai, W. Zhu, Y. Chen, Amphiphilic toothbrushlike copolymers based on poly(ethylene glycol) and poly (ε-caprolactone) as drug carriers with enhanced properties, Biomacromolecules 11 (2010) 1331–1338, https://doi.org/10.1021/bm100116g.
[18] A. Kakkar, G. Traverso, O.C. Farokhzad, R. Weissleder, R. Langer, Evolution of macromolecular complexity in drug delivery systems, Nat. Rev. Chem. 1 (2017), https://doi.org/10.1038/s41570-017-0063.
[19] P.R. Rodrigues, R.P. Vieira, Advances in atom-transfer radical polymerization for drug delivery applications, Eur. Polym. J. 115 (2019) 45–58, https://doi.org/10.1016/j.eurpolymj.2019.03.023.
[20] D.P. Yang, M.N.N.L. Oo, G.R. Deen, Z. Li, X.J. Loh, Nano-star-shaped polymers for drug delivery applications, Macromol. Rapid Commun. 38 (2017), https://doi.org/10.1002/marc.201700410.
[21] R. Aksakal, C. Mertens, M. Soete, N. Badi, F. Du Prez, Applications of discrete synthetic macromolecules in life and materials science: Recent and future trends, Adv. Sci. 8 (2021), https://doi.org/10.1002/advs.202004038.
[22] J.F. Lutz, M. Ouchi, D.R. Liu, M. Sawamoto, Sequence-controlled polymers, Science (1979) 341 (2013). DOI: 10.1126/science.1238149.
[23] K. Zhang, Y. Wang, W. Zhu, X. Li, Z. Shen, Synthesis, characterization, and micellization of PCL-g-PEG copolymers by combination of ROP and "click" chemistry via "graft onto" method, J. Polym. Sci. A Polym. Chem. 50 (2012) 2045–2052, https://doi.org/10.1002/pola.25979.
[24] S. Khoee, A. Kavand, F. Hashemi Nasr, Preparation of new dendrimer-like star-shaped amphiphilic poly(ethylene glycol)-poly(ϵ-caprolactone) copolymers for biocompatible and high-efficiency curcumin delivery, Polym Int 64 (2015) 1191–1201. DOI: 10.1002/pi.4896.
[25] R. Bruni, P. Possenti, C. Bordignon, M. Li, S. Ordanini, P. Messa, M.P. Rastaldi, F. Cellesi, Ultrasmall polymeric nanocarriers for drug delivery to podocytes in kidney glomerulus, J. Control. Release 255 (2017) 94–107, https://doi.org/10.1016/j.jconrel.2017.04.005.
[26] I. Proietti Silvestri, F. Cellesi, AGET ATRP of Poly[poly(ethylene glycol) methyl ether methacrylate] Catalyzed by Hydrophobic Iron(III)-Porphyrins, Macromol Chem Phys 216 (2015) 2032–2039. DOI: 10.1002/macp.201500277.
[27] X. Zhang, Z. Zhang, X. Su, H. Dong, Z. Zhong, R. Zhuo, Synthesis of amphiphilic comb-shape copolymers via ring-opening polymerization of a macromonomer, Macromol. Chem. Phys. 216 (2015) 1712–1717, https://doi.org/10.1002/macp.201500161.
[28] C. Von Der Ehe, K. Kempe, M. Bauer, A. Baumgaertel, M.D. Hager, D. Fischer, U. S. Schubert, Star-shaped block copolymers by copper-catalyzed azide-alkyne cycloaddition for potential drug delivery applications, Macromol. Chem. Phys. 213 (2012) 2146–2156, https://doi.org/10.1002/macp.201200307.
[29] S. Petrova, I. Kolev, S. Miloshev, M.D. Apostolova, R. Mateva, Synthesis of amphiphilic [PEO(PCL) 2] triarm star-shaped block copolymers: A promising system for in cell delivery, J. Mater. Sci. - Mater. Med. 23 (2012) 1225–1234, https://doi.org/10.1007/s10856-012-4592-8.
[30] Y. Zhou, L. Li, W. Chen, D. Li, N. Zhou, J. He, P. Ni, Z. Zhang, X. Zhu, A twin-tailed tadpole-shaped amphiphilic copolymer of poly(ethylene glycol) and cyclic poly (ϵ-caprolactone): Synthesis, self-assembly and biomedical applications, Polym. Chem. 9 (2018) 4343–4353, https://doi.org/10.1039/c8py00022k.
[31] X. Sun, G. Wang, H. Zhang, S. Hu, X. Liu, J. Tang, Y. Shen, The blood clearance kinetics and pathway of polymeric micelles in cancer drug delivery, ACS Nano 12 (2018) 6179–6192, https://doi.org/10.1021/acsnano.8b02830.
[32] A.D. Ayub, H.I. Chiu, S.N.A. Mat Yusuf, E. Abd Kadir, S.H. Ngalim, V. Lim, Biocompatible disulphide cross-linked sodium alginate derivative nanoparticles for oral colon-targeted drug delivery, Artif. Cells Nanomed. Biotechnol. 47 (2019) 353–369, https://doi.org/10.1080/21691401.2018.1557672.
[33] B. Korthals, M.C. Morant-Miñana, M. Schmid, S. Mecking, Functionalization of polymer nanoparticles by thiol-ene addition, Macromolecules 43 (2010) 8071–8078, https://doi.org/10.1021/ma100966w.
[34] M.H. Dufresne, M.A. Gauthier, J.C. Leroux, Thiol-functionalized polymeric micelles: From molecular recognition to improved mucoadhesion, Bioconjug. Chem. 16 (2005) 1027–1033, https://doi.org/10.1021/bc050007b.
[35] S. Ordanini, W. Celentano, A. Bernardi, F. Cellesi, Mannosylated brush copolymers based on poly(ethylene glycol) and poly(ε-caprolactone) as multivalent lectin-binding nanomaterials, Beilstein J. Nanotechnol. 10 (2019) 2192–2206, https://doi.org/10.3762/bjnano.10.212.
[36] V. Ladmiral, G. Mantovani, G.J. Clarkson, S. Cauet, J.L. Irwin, D.M. Haddleton, Synthesis of neoglycopolymers by a combination of "click chemistry" and living radical polymerization, J. Am. Chem. Soc. 128 (2006) 4823–4830, https://doi.org/10.1021/ja058364k.
[37] C.R. Becer, M.I. Gibson, J. Geng, R. Ilyas, R. Wallis, D.A. Mitchell, D.M. Haddleton, High-affinity glycopolymer binding to human DC-SIGN and disruption of DC-SIGN interactions with HIV envelope glycoprotein, J. Am. Chem. Soc. 132 (2010) 15130–15132, https://doi.org/10.1021/ja1056714.
[38] L.A. Lane, Physics in nanomedicine: Phenomena governing the in vivo performance of nanoparticles, Appl. Phys. Rev. 7 (2020), https://doi.org/10.1063/1.5052455.
[39] G. Pasut, Grand challenges in nano-based drug delivery, Front. Med. Technol. 1 (2019), https://doi.org/10.3389/fmedt.2019.00001.
[40] N. Hock, G.F. Racaniello, S. Aspinall, N. Denora, V.V. Khutoryanskiy, A. Bernkop-Schnürch, Thiolated nanoparticles for biomedical applications: Mimicking the workhorses of our body, Adv. Sci. 9 (2022), https://doi.org/10.1002/advs.202102451.
[41] G. Yilmaz, C.R. Becer, Glycopolymer code: Programming synthetic macromolecules for biological targeting, Macromol. Chem. Phys. 221 (2020), https://doi.org/10.1002/macp.202000006.
[42] J. Li, K. Kataoka, Chemo-physical strategies to advance the in vivo functionality of targeted nanomedicine: The next generation, J. Am. Chem. Soc. 143 (2021) 538–559, https://doi.org/10.1021/jacs.0c09029.
[43] K. Matyjaszewski, Advanced materials by atom transfer radical polymerization, Adv. Mater. 30 (2018), https://doi.org/10.1002/adma.201706441.
[44] N.V. Tsarevsky, W.A. Braunecker, K. Matyjaszewski, Electron transfer reactions relevant to atom transfer radical polymerization, J. Organomet. Chem. 692 (2007) 3212–3222, https://doi.org/10.1016/j.jorganchem.2007.01.051.
[45] O. Nuyken, S.D. Pask, Ring-opening polymerization-An introductory review, Polymers (Basel) 5 (2013) 361–403, https://doi.org/10.3390/polym5020361.
[46] S. Dworakowska, F. Lorandi, A. Gorczyński, K. Matyjaszewski, Toward green atom transfer radical polymerization: Current status and future challenges, Adv. Sci. 9 (2022), https://doi.org/10.1002/advs.202106076.
[47] X.W. Wei, C.Y. Gong, M.L. Gou, S.Z. Fu, Q.F. Guo, S. Shi, F. Luo, G. Guo, L.Y. Qiu, Z.Y. Qian, Biodegradable poly(ε-caprolactone)-poly(ethylene glycol) copolymers as drug delivery system, Int. J. Pharm. 381 (2009) 1–18, https://doi.org/10.1016/j.ijpharm.2009.07.033.
[48] A. Al Samad, Y. Bakkour, F. Coumes, F. El Omar, J. Coudane, B. Nottelet, From nanospheres to micelles: Simple control of PCL-g-PEG copolymers' amphiphilicity through thiol-yne photografting, Polym. Chem. 6 (2015) 5093–5102, https://doi.org/10.1039/c5py00391a.
[49] K.S. Shalaby, M.E. Soliman, G. Bonacucina, M. Cespi, G.F. Palmieri, O.A. Sammour, A.A. El Shamy, L. Illum, L. Casettari, Nanoparticles based on linear and star-shaped poly(Ethylene Glycol)-poly(ε-Caprolactone) copolymers for the delivery of antitubulin drug, Pharm. Res. 33 (2016) 2010–2024, https://doi.org/10.1007/s11095-016-1939-8.
[50] I. Ali, F. Kareem, S. Rahim, S. Perveen, S. Ahmed, M.R. Shah, M.I. Malik, Architecture based selectivity of Amphiphilic block copolymers of poly(ethylene oxide) and poly(ε-caprolactone) for drug delivery, React. Funct. Polym. 150 (2020), https://doi.org/10.1016/j.reactfunctpolym.2020.104553.
[51] F. Moncalvo, M.I. Martinez Espinoza, F. Cellesi, Nanosized delivery systems for therapeutic proteins: Clinically validated technologies and advanced development strategies, Front. Bioeng. Biotechnol. 8 (2020), https://doi.org/10.3389/fbioe.2020.00089.
[52] G. Pasut, Polymers for protein conjugation, Polymers (Basel) 6 (2014) 160–178, https://doi.org/10.3390/polym6010160.
[53] A.S. Mikhail, C. Allen, Poly(ethylene glycol)- b -poly(ε-caprolactone) micelles containing chemically conjugated and physically entrapped docetaxel: Synthesis, characterization, and the influence of the drug on micelle morphology, Biomacromolecules 11 (2010) 1273–1280, https://doi.org/10.1021/bm100073s.
[54] F. Moncalvo, E. Lacroce, G. Franzoni, A. Altomare, E. Fasoli, G. Aldini, A. Sacchetti, F. Cellesi, Selective protein conjugation of poly(glycerol monomethacrylate) and poly(polyethylene glycol methacrylate) with tunable topology via reductive amination with multifunctional ATRP initiators for activity preservation, Macromolecules 55 (2022) 7454–7468, https://doi.org/10.1021/acs.macromol.2c00783.
[55] F. Moncalvo, E. Lacroce, G. Franzoni, A. Altomare, E. Fasoli, G. Aldini, A. Sacchetti, F. Cellesi, Protein-friendly atom transfer radical polymerisation of glycerol (monomethacrylate) in buffer solution for the synthesis of a new class of polymer bioconjugates, React. Funct. Polym. 175 (2022), https://doi.org/10.1016/j.reactfunctpolym.2022.105264.
[56] P. De Leonardis, F. Cellesi, N. Tirelli, Tuning the properties of hybrid SiO2/ poly (glycerol monomethacrylate) nanoparticles for enzyme nanoencapsulation, Colloids Surf. A Physicochem. Eng. Asp. 580 (2019), https://doi.org/10.1016/j.colsurfa.2019.123734.
[57] L. Ragupathy, D.G. Millar, N. Tirelli, F. Cellesi, An orthogonal click-chemistry approach to design poly(glycerol monomethacrylate)-based nanomaterials for controlled immunostimulation, Macromol. Biosci. 14 (2014) 1528–1538, https://doi.org/10.1002/mabi.201400146.
[58] T. Eom, A. Khan, Disulfides as mercapto-precursors in nucleophilic ring opening reaction of polymeric epoxides: Establishing equimolar stoichiometric conditions in a thiol-epoxy "click" reaction, Chem. Commun. 56 (2020) 7419–7422, https://doi.org/10.1039/d0cc02601h.
[59] A.S. Goldmann, M. Glassner, A.J. Inglis, C. Barner-Kowollik, Post-functionalization of polymers via orthogonal ligation chemistry, Macromol. Rapid Commun. 34 (2013) 810–849, https://doi.org/10.1002/marc.201300017.
[60] W. Celentano, M. Pizzocri, F. Moncalvo, F. Pessina, M. Matteoli, F. Cellesi, L. Passoni, Functional poly(ϵ-caprolactone)/poly(ethylene glycol) copolymers with complex topologies for doxorubicin delivery to a proteinase-rich tumor environment, ACS Appl. Polym. Mater. 4 (2022) 8043–8056, https://doi.org/10.1021/acsapm.2c00897.
[61] F. Cellesi, N. Tirelli, J.A. Hubbell, Towards a fully-synthetic substitute of alginate: Development of a new process using thermal gelation and chemical cross-linking, Biomaterials 25 (2004) 5115–5124, https://doi.org/10.1016/j.biomaterials.2003.12.015.
[62] G. Camana, M. Tavano, M. Li, F. Castiglione, F. Rossi, F. Cellesi, Design of functional pluronic-based precursors for tailoring hydrogel thermoresponsiveness

and cell-adhesive properties, Materials 16 (2023), https://doi.org/10.3390/ma16072749.
[63] S. Summonte, G.F. Racaniello, A. Lopedota, N. Denora, A. Bernkop-Schnürch, Thiolated polymeric hydrogels for biomedical application: Cross-linking mechanisms, J. Control. Release 330 (2021) 470–482, https://doi.org/10.1016/j.jconrel.2020.12.037.
[64] C. Federer, M. Kurpiers, A. Bernkop-Schnürch, Thiolated chitosans: A multi-talented class of polymers for various applications, Biomacromolecules 22 (2021) 24–56, https://doi.org/10.1021/acs.biomac.0c00663.
[65] C. Leichner, M. Jelkmann, A. Bernkop-Schnürch, Thiolated polymers: Bioinspired polymers utilizing one of the most important bridging structures in nature, Adv. Drug Deliv. Rev. 151–152 (2019) 191–221, https://doi.org/10.1016/j.addr.2019.04.007.
[66] R. Grosso, M.V. De-Paz, Thiolated-polymer-based nanoparticles as an avant-garde approach for anticancer therapies—reviewing thiomers from chitosan and hyaluronic acid, Pharmaceutics 13 (2021), https://doi.org/10.3390/pharmaceutics13060854.
[67] T.M.M. Ways, S.K. Filippov, S. Maji, M. Glassner, M. Cegłowski, R. Hoogenboom, S. King, W.M. Lau, V.V. Khutoryanskiy, Mucus-penetrating nanoparticles based on chitosan grafted with various non-ionic polymers: Synthesis, structural characterisation and diffusion studies, J. Colloid Interface Sci. 626 (2022) 251–264, https://doi.org/10.1016/j.jcis.2022.06.126.
[68] E. Rostami, Recent achievements in sodium alginate-based nanoparticles for targeted drug delivery, Polym. Bull. 79 (2022) 6885–6904, https://doi.org/10.1007/s00289-021-03781-z.
[69] M. Sajjad, M.I. Khan, S. Naveed, S. Ijaz, O.S. Qureshi, S.A. Raza, G. Shahnaz, M. F. Sohail, Folate-functionalized thiomeric nanoparticles for enhanced docetaxel cytotoxicity and improved oral bioavailability, AAPS PharmSciTech 20 (2019), https://doi.org/10.1208/s12249-019-1297-z.
[70] F. Prüfert, U. Hering, S. Zaichik, N.M.N. Le, A. Bernkop-Schnürch, Synthesis and in vitro characterization of a preactivated thiolated acrylic acid/acrylamide-methylpropane sulfonic acid copolymer as a mucoadhesive sprayable polymer, Int. J. Pharm. 583 (2020), https://doi.org/10.1016/j.ijpharm.2020.119371.
[71] S. Duggan, W. Cummins, O. O' Donovan, H. Hughes, E. Owens, Thiolated polymers as mucoadhesive drug delivery systems, European Journal of Pharmaceutical Sciences 100 (2017) 64–78. DOI: 10.1016/j.ejps.2017.01.008.
[72] A. Štorha, E.A. Mun, V.V. Khutoryanskiy, Synthesis of thiolated and acrylated nanoparticles using thiol-ene click chemistry: Towards novel mucoadhesive materials for drug delivery, RSC Adv. 3 (2013) 12275–12279, https://doi.org/10.1039/c3ra42093k.
[73] E.O. Shatabayeva, D.B. Kaldybekov, L. Ulmanova, B.A. Zhaisanbayeva, E.A. Mun, Z.A. Kenessova, S.E. Kudaibergenov, V.V. Khutoryanskiy, Enhancing mucoadhesive properties of gelatin through chemical modification with unsaturated anhydrides, Biomacromolecules 25 (2024) 1612–1628, https://doi.org/10.1021/acs.biomac.3c01183.
[74] E. Taipaleenmäki, B. Städler, Recent advancements in using polymers for intestinal mucoadhesion and mucopenetration, Macromol. Biosci. 20 (2020), https://doi.org/10.1002/mabi.201900342.
[75] B.Á. Szilágyi, A. Mammadova, B. Gyarmati, A. Szilágyi, Mucoadhesive interactions between synthetic polyaspartamides and porcine gastric mucin on the colloid size scale, Colloids Surf. B Biointerfaces 194 (2020), https://doi.org/10.1016/j.colsurfb.2020.111219.
[76] S.J. Hunter, M.H. Abu Elella, E.C. Johnson, L. Taramova, E.E. Brotherton, S.P. Armes, V. V. Khutoryanskiy, M.J. Smallridge, Mucoadhesive pickering nanoemulsions via dynamic covalent chemistry, J Colloid Interface Sci 651 (2023) 334–345. DOI: 10.1016/j.jcis.2023.07.162.
[77] Y. Yamada, Dimerization of doxorubicin causes its precipitation, ACS Omega 5 (2020) 33235–33241, https://doi.org/10.1021/acsomega.0c04925.
[78] J. Barthelmes, S. Dnnhaupt, J. Hombach, A. Bernkop-Schnrch, Thiomer nanoparticles: Stabilization via covalent cross-linking, Drug Deliv. 18 (2011) 613–619, https://doi.org/10.3109/10717544.2011.621986.
[79] P. Eyer, F. Worek, D. Kiderlen, G. Sinko, A. Stuglin, V. Simeon-Rudolf, E. Reiner, Molar absorption coefficients for the reduced Ellman reagent: reassessment q, n.d. www.elsevier.com/locate/yabio.
[80] K. Kim, K. Kim, J.H. Ryu, H. Lee, Chitosan-catechol: A polymer with long-lasting mucoadhesive properties, Biomaterials 52 (2015) 161–170, https://doi.org/10.1016/j.biomaterials.2015.02.010.
[81] G. Kocak, G. Solmaz, C. Tuncer, V. Bütün, Modification of glycidyl methacrylate based block copolymers and their aqueous solution behaviours, Eur. Polym. J. 110 (2019) 364–377, https://doi.org/10.1016/j.eurpolymj.2018.11.046.
[82] K.A. Günay, P. Theato, H.A. Klok, Standing on the shoulders of hermann staudinger: Post-polymerization modification from past to present, J. Polym. Sci. A Polym. Chem. 51 (2013) 1–28, https://doi.org/10.1002/pola.26333.
[83] M.C. Stuparu, A. Khan, Thiol-epoxy "click" chemistry: Application in preparation and postpolymerization modification of polymers, J. Polym. Sci. A Polym. Chem. 54 (2016) 3057–3070, https://doi.org/10.1002/pola.28195.
[84] E.M. Muzammil, A. Khan, M.C. Stuparu, Post-polymerization modification reactions of poly(glycidyl methacrylate)s, RSC Adv. 7 (2017) 55874–55884, https://doi.org/10.1039/c7ra11093f.
[85] S. De, A. Khan, Efficient synthesis of multifunctional polymers via thiol-epoxy "lick" chemistry, Chem. Commun. 48 (2012) 3130–3132, https://doi.org/10.1039/c2cc30434a.
[86] M. Rodlert, E. Harth, I. Rees, C.J. Hawker, End-group fidelity in nitroxide-mediated living free-radical polymerizations, J. Polym. Sci. A Polym. Chem. 38 (2000) 4749–4763, https://doi.org/10.1002/1099-0518(200012)38:1+<4749::aid-pola140>3.0.co;2-d.
[87] E. Sah, H. Sah, Recent trends in preparation of poly(lactide-co-glycolide) nanoparticles by mixing polymeric organic solution with antisolvent, J. Nanomater. 2015 (2015), https://doi.org/10.1155/2015/794601.
[88] J. Cheng, B.A. Teply, I. Sherifi, J. Sung, G. Luther, F.X. Gu, E. Levy-Nissenbaum, A. F. Radovic-Moreno, R. Langer, O.C. Farokhzad, Formulation of functionalized PLGA-PEG nanoparticles for in vivo targeted drug delivery, Biomaterials 28 (2007) 869–876, https://doi.org/10.1016/j.biomaterials.2006.09.047.
[89] D.H. Kim, S.Y. Kim, Scaling laws for block copolymer surface micelles, J. Phys. Chem. Lett. 13 (2022) 5380–5386, https://doi.org/10.1021/acs.jpclett.2c00979.
[90] S. Förster, M. Zisenis, E. Wenz, M. Antonietti, Micellization of strongly segregated block copolymers, J. Chem. Phys. 104 (1996) 9956–9970, https://doi.org/10.1063/1.471723.
[91] R. Singh, J.W. Lillard, Nanoparticle-based targeted drug delivery, Exp. Mol. Pathol. 86 (2009) 215–223, https://doi.org/10.1016/j.yexmp.2008.12.004.
[92] K. Mfoafo, R. Mittal, A. Eshraghi, Y. Omidi, H. Omidian, Thiolated polymers: An overview of mucoadhesive properties and their potential in drug delivery via mucosal tissues, J. Drug Deliv. Sci. Technol. 85 (2023), https://doi.org/10.1016/j.jddst.2023.104596.
[93] M. Fu, S.K. Filippov, A.C. Williams, V.V. Khutoryanskiy, On the mucoadhesive properties of synthetic and natural polyampholytes, J. Colloid Interface Sci. 659 (2024) 849–858, https://doi.org/10.1016/j.jcis.2023.12.176.